Accepted Manuscript

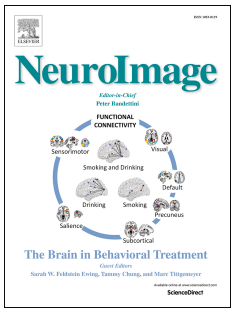

Neural substrates of cognitive reserve in Alzheimer's disease spectrum and normal aging

Dong Hyuk Lee, Peter Lee, Sang Won Seo, Jee Hoon Roh, Minyoung Oh, Jungsu S. Oh, Seung Jun Oh, Jae Seung Kim, Yong Jeong

PII: S1053-8119(18)32134-7

DOI: https://doi.org/10.1016/j.neuroimage.2018.11.053

Reference: YNIMG 15458

To appear in: *NeuroImage*

Received Date: 6 November 2018

Revised Date: 27 November 2018

Accepted Date: 28 November 2018

Please cite this article as: Lee, D.H., Lee, P., Seo, S.W., Roh, J.H., Oh, M., Oh, J.S., Oh, S.J., Kim, J.S., Jeong, Y., Neural substrates of cognitive reserve in Alzheimer's disease spectrum and normal aging, *NeuroImage* (2018), doi: https://doi.org/10.1016/j.neuroimage.2018.11.053.

Neural substrates of cognitive reserve in Alzheimer's disease spectrum and normal aging

Dong Hyuk Lee[a,b], Peter Lee[b,f], Sang Won Seo[c], Jee Hoon Roh[d], Minyoung Oh[e], Jungsu S. Oh[e], Seung Jun Oh[e], Jae Seung Kim[e], Yong Jeong[a,b,f,*]

[a]Graduate School of Medical Science and Engineering and [b]KI for Health Science and Technology, Korea Advanced Institute of Science and Technology, Daejeon, Republic of Korea

[c]Department of Neurology, Samsung Medical Center, Sunkyunkwan University School of Medicine, Seoul, Republic of Korea

[d]Department of Neurology and [e]Nuclear Medicine, Asan Medical Center, University of Ulsan College of Medicine, Seoul, Republic of Korea

[f]Department of Bio and Brain Engineering, Korea Advanced Institute of Science and Technology, Daejeon, Republic of Korea.

Dong Hyuk Lee: rapha_ldh@kaist.ac.kr

* Corresponding author: Yong Jeong, Department of Bio and Brain Engineering, KAIST, Daehak-ro 291, Yuseong-gu, Daejeon, 34141, Republic of Korea. (E-mail: yong@kaist.ac.kr)

Abstract

The concept of cognitive reserve (CR) originated from discrepancies between the degree of brain pathology and the severity of clinical manifestations. CR has been characterized through CR proxies, such as education and occupation complexity; however, such approaches have inherent limitations. Although several methods have been developed to overcome these limitations, they fail to reflect the entire Alzheimer's disease (AD) pathology. Meanwhile, graph theory analysis, one of most powerful and flexible approaches, have established remarkable network properties of the brain. The functional and structural brain networks are damaged in neurodegenerative diseases. Therefore, network analysis has been applied to clarify the characteristics of the disease or give insight. Here, using multimodal neuroimaging, we propose an intuitive model to estimate CR based on its original definition, and explore the neural substrates of CR from the perspective of networks and functional connectivity. A total of 87 subjects (21 AD, 32 mild cognitive impairment, and 34 normal aging) underwent tau and amyloid PET, 3D T1-weighted MR, and resting-state fMRI. We hypothesized CR as a residual of actual cognitive performance and expected performance to be related to quantitative factors, such as AD pathology, demographics, and a genetic factor. Then, we correlated this marker using education and occupation complexity as conventional CR proxies. We validated this marker by testing whether it would modulate the effect of brain pathology on memory function. To examine the neural substrates associated with CR, we performed graph analysis to investigate the association between the CR marker and network measures at different granularities in total subjects, AD spectrum and normal aging, respectively. The CR marker from our model was well associated with education and occupation complexity. More directly, the CR marker was revealed to modify the relationship between brain pathology and memory function among AD spectrum. The CR marker was correlated with the global efficiency of the entire network, nodal clustering

coefficient, and local efficiency of the right middle-temporal pole. In connectivity analysis, one cluster of edges centered on right middle-temporal pole was significantly correlated with the CR marker. In subgroup analysis, the network measures of right middle-temporal pole still correlated with the CR marker among AD spectrum. However, right precentral gyrus was revealed to be associated with the CR marker in normal aging. This study demonstrates that our intuitive model using multimodal neuroimaging and network perspective adequately and comprehensively captures CR. From a network perspective, CR is associated with the capacity to process information efficiently in the brain. The right middle-temporal pole was revealed to be a pivotal neural substrate of CR in AD spectrum. These findings foster understanding of AD and will be useful to help identify individuals with vulnerability or resistance to AD pathology, and characterize patients for intervention or drug trials.

Keywords: Cognitive reserve, multimodal neuroimaging, brain network, Alzheimer's disease

1. Introduction

The concept of cognitive reserve (CR) derives from observations of discrepancies between the extent of brain pathology and the severity of clinical manifestations (Katzman et al., 1988). CR has been proposed as a protective factor that modifies the effect of brain pathology on cognitive performance (Stern, 2002). Researchers have defined CR as the ability to optimize cognitive performance through differential recruitment of brain structures or networks (Stern, 2002). Two mechanisms have been suggested to contribute to CR: neural reserve and neural compensation (Stern, 2012; Stern et al., 2005). Neural reserve refers to the differential activation of pre-existing less vulnerable resources, while neural compensation denotes the recruitment of compensatory networks when pathology afflicts the primary task-related network.

The concept of CR has been tested primarily in patients with Alzheimer's disease (AD). Epidemiological studies suggest that cognitive exposures through lifespan, including education (Hall et al., 2007; Meng and D'Arcy, 2012), occupation (Adam et al., 2013; Richards and Sacker, 2003), and leisure activities (Fabrigoule et al., 1995; Scarmeas et al., 2001) can delay the onset of cognitive impairment by enhancing CR. Therefore, these features have been widely accepted as CR proxies. Meanwhile, recent advances in imaging techniques permit visualization of the level of AD pathology, such as the accumulation of Aβ plaques and tau tangles, and neuronal degeneration; thus, these characteristics have been introduced as CR correlates (Braak et al., 1998; Serrano-Pozo et al., 2011). Greater CR is associated with lower perfusion (Stern et al., 1992), hypometabolism (Ewers et al., 2013), and more cortical atrophy (Liu et al., 2012) in parietotemporal areas, as well as with more tau (Hoenig et al., 2017) and Aβ (Kemppainen et al., 2008) aggregation at the same level of clinical severity, indicating that patients with higher CR tolerate more AD pathology before

cognitive impairments appear.

However, proxies such as education, occupation or leisure activities have limitations in that they are not accurate or dynamic, and the same value does not assure the same degree of experience across individuals. These proxies are also highly correlated among themselves (Zahodne et al., 2013). To overcome these limitations, several models have been suggested, including a latent variable model in which education was already assigned to the demographic factor (Reed et al., 2010), a model using a w-score method (van Loenhoud et al., 2017), and a residual model (Habeck et al., 2016). Although these correspond to the original definition of CR, namely the discrepancy between actually measured and estimated cognitive performance from the pathologic burden, they fail to reflect the overall AD pathology (not only gray-matter atrophy but also Aβ and tau) in the model.

Meanwhile, graph theoretic approach has identified remarkable network properties of the brain, such as small-worldness (Watts and Strogatz, 1998), hierarchical modularity (Meunier et al., 2009) and hub organization (van den Heuvel and Sporns, 2013). The functional brain networks are related to predict inter-individual variability and intelligence (Langer et al., 2012; Mueller et al., 2013). These brain networks are revealed to be damaged in psychiatric or neurodegenerative diseases (Filippi et al., 2017; Liu et al., 2008). Therefore, a network perspective of graph theory has been utilized to clarify the characteristics of the disease or give insight into it. In respect to CR, even though CR is known to be associated with the ability to optimize or recruit brain networks differentially, few studies have focused on CR from the network perspective.

In the present study, we propose an intuitive model to conceptualize CR based on its original definition, using multimodal imaging including tau and amyloid PET and T1 images. Then, we validate our CR marker by comparison with conventional CR proxies and test whether it modulates the relationship between brain pathology and memory function. Finally, we

investigate how network topological characteristics across different granularities correlate with CR, to reveal the core substrates of CR.

2. Materials and Methods

2. 1. Study population

Eighty-seven subjects (21 AD, 32 amnestic MCI, 34 normal aging) were recruited at the memory disorder clinic in the Department of Neurology at the Asan Medical Center (AMC) and the Samsung Medical Center (SMC) in Seoul, South Korea. Each participant received MRI, resting-state fMRI, tau (THK-5351) and amyloid (florbetaben) PET, clinical interviews, and comprehensive neuropsychological assessments. All AD subjects fulfilled the criteria for a clinical diagnosis of AD according to the National Institute of Neurological and Communicative Disorders and Stroke and Alzheimer's disease and Related Disorders Association (McKhann et al., 2011) and those with MCI met the Petersen's criteria (Petersen et al., 1999). Subjects with AD and MCI were amyloid positive as determined by brain amyloid plaque load (BAPL score) ≥2 (Sabri et al., 2015). Normal aging is defined as an elderly with free of neurological disease, a clinical dementia rating (CDR) 0 and a Mini-Mental State Examination (MMSE) score higher than 27. Exclusion criteria were 1) meeting core clinical criteria for another form of dementia or variants of clinical AD; 2) significant medical illnesses or substance abuse that could influence cognitive function; 3) history of major systemic, psychiatric, or neurological disorder; or 4) presence of clinically significant cerebrovascular disease. The Institutional Review Board of the AMC and SMC approved the study and all subjects (or caregivers) provided informed consent for research according to the guidelines outlined in the Declaration of Helsinki.

2. 2. Neuropsychological assessment and CR surrogate markers

We measured cognitive performance as a global composite score that combined 14 neuropsychological test scores across multiple cognitive domains; this was based on approaches adopted in previous studies (Ahn et al., 2010; Jahng. et al., 2015). The memory domain consisted of immediate recall (sum of 3 trials, 0-12 points/trial), delayed recall (0-12 points), and recognition test (True positive + 12 – False positive, 0-24 points) of the Seoul Verbal Learning Test-Elderly's version (SVLT-E) and the immediate recall (sum of 18 scoring units, 0-2 points/unit) , delayed recall (sum of 18 scoring units, 0-2 points/unit), and recognition test (True positive + 12 – False positive, 0–24 points) of Rey Complex Figure Test (RCFT) (Kang and Na, 2003; Meyers and Meyers, 1995). Executive function was assessed via the contrasting program (a test for response inhibition, 0-20 points), Go-No-Go test (a pass/fail test principle using two boundary conditions, 0-20 points), category fluency (correct responses to presented category, such as animal and supermarket within 1 minute), and phonemic fluency components of the Controlled Oral Ward Association Test (correct responses to presented phonemes, such as Letter M and S within 1 minute) (Benton and Hamsher, 1989). To assess visuospatial function, we employed the score of the RCFT copying task (sum of 18 scoring units, 0-2 points/unit). Attention was assessed via scores on the forward (sum of items correctly repeated forwards, 0-9 points) and backward (sum of items correctly repeated backwards, 0-8 points) Digit Span Test (DST) (Lezak, 1995). Finally, the language domain was assessed using the Korean-Boston Naming Test (K-BNT) (correct naming of 60 line drawings, 1 point /drawing) (Kim and Na, 1999). We defined a global cognitive composite score as the average of total raw scores in the five domains.

We used years of education and occupation complexity as two representative CR proxies. Education is widely accepted as the most relevant CR proxy to date. Occupation complexity was measured by Dictionary of Occupational Titles (DOT) ratings (Labor., 1977). The DOT classifies occupations based on a 9-digit code. The fourth, fifth, and sixth digits represent

occupational complexity with each of the three domains being data, people and things (Ex. 092.227-010 for primary school teacher. In this case, 2 (4^{th}) represents occupational complexity with data, 2 (5^{th}) represents complexity with people and 7 (6^{th}) means complexity in things.). In DOT, the lower score indicates higher occupational complexity, denoting higher CR.

2. 3. Image acquisition

We obtained T1-weighted MR images (repetition time (TR) = 6.8 ms; echo time (TE) = 3.1 ms; flip angle = 9°; field of view = 270 x 252 mm^2; voxel size = 1.11 x 1.11 x 1.2 mm^3; slice number = 170 for AMC and TR = 9.9 ms; TE = 4.6 ms; flip angle = 8°; field of view = 240 x 240 mm^2; voxel size = 1.0 x 1.0 x 0.5 mm^3; slice number = 360 for SMC), using a 3T Philips Intera Achieva (Philips Healthcare, Eindhoven, The Netherlands). T2*-weighted MR images for resting state fMRI (TR = 3000 ms; TE = 30 ms; flip angle = 90°; field of view = 212 x 212 mm^2; voxel size = 3.3 x 3.3 x 3.3 mm^3; slice number = 48 for AMC and TR = 3000 ms; TE = 35 ms; flip angle = 90°; field of view = 220 x 220 mm^2; voxel size = 1.72 x 1.72 x 4 mm^3; slice number=35 for SMC) were acquired using a gradient echo-planar imaging pulse sequence.

We used a Discovery 690, 710, and 690 Elite PET/CT scanner at AMC and a Discovery STE PET/CT scanner at SMC (GE Healthcare, Milwaukee, USA) with the same protocol at both centers. Tau PET images were acquired for 20 minutes, starting 50 minutes after an intravenous bolus injection of 185 ± 18.5 MBq of 18F-THK5351, which binds to the aggregated tau of paired helical filaments. Amyloid PET images were acquired for 20 minutes, starting 90 minutes after an intravenous bolus injection of 300 ± 30 MBq of 18F-florbetaben. Before the PET scan, we applied a head stabilizer to minimize head motion and acquired brain CT images for attenuation correction. Using the ordered-subsets expectation maximization algorithm (iteration = 4, subset = 16), three-dimensional PET images were

reconstructed with voxel size 2.0 × 2.0 × 3.27 mm^3. To accommodate data from different PET/CT scanners, we applied a three-dimensional Hoffman phantom-based PET harmonization method previously reported (Joshi et al., 2009).

2. 4. Data preprocessing

Individual tau and amyloid PET images were co-registered onto the individual T1-weighted image and normalized into MNI standard space. Preprocessed images were smoothed (6 mm full-width half-maximum Gaussian kernel). Standard uptake value (SUV) images (40–60 min) were also created for tau and amyloid PET. SUV was defined as the radioactivity concentration (MBq/mL) divided by injected dose (MBq)/patient's weight (kg) (Chiotis et al., 2016). Standard uptake value ratio (SUVR) images were calculated for all individuals, using cerebellar Gray Matter (GM) — extracted from an automated anatomical labelling (AAL) atlas — as a reference. All preprocessing was conducted using SPM12 (Wellcome Trust Centre for Neuroimaging, University College London) and MATLAB R2014b (The Mathworks, Natick, MA).

In fMRI preprocessing, we discarded the first five EPI volumes because of signal stabilization. We then performed pre-processing for the resting state fMRI including slice-timing correction, realignment for motion correction, co-registration to T1-weighted images, linear detrending, nuisance covariate regression for six motion parameters, segregation of white matter and CSF, spatial normalization into the MNI template, and smoothing (6 mm FWHM). Additionally, all preprocessed images were band-pass filtered (0.01–0.08 Hz). We also confirmed that there was no excessive head motion in preprocessed images (translation >2 mm, rotation >2°).

To extract cortical thickness, T1 MR images underwent preprocessing steps with Freesurfer

6.0 (https://surfer.nmr.mgh.harvard.edu). These steps included intensity normalization, registration, skull stripping, segmentation, tessellation of white matter, automated topology correction, surface registration, and cortical parcellation (Chung et al., 2017). In addition, we performed manual correction for all segmentation images, focusing on the dura of skull and CSF space. Finally, we extracted thickness values in 68 bilateral Desikan-Killiany ROIs to calculate a global cortical thickness value per subject (Desikan et al., 2006). Total intracranial volume (TIV) was defined as the total volume of the cranium; this was obtained by summing volumes of gray matter, white matter, and CSF. SPM12 implemented in MATLAB 2014b was used to segment each tissue in native space using probability maps.

2. 5. An intuitive model to estimate CR

Based on the original definition of CR, we hypothesized CR as a residual of actual cognitive performance and expected performance; the latter was defined based on pathology, demographics, a genetic factor, and TIV (Fig. 1). The residual concept to quantify CR has been applied in previous studies. However, all previous works just covered structural measures such as cortical volume, thickness, white matter hyper intensity and tract using standard MR assessments. In contrast, our model focused more on the reflection of overall AD neuropathology. According to the trajectory of AD biomarkers, two major proteinopathies — Aβ and tau — may be initiated sequentially or independently decades before the onset of AD. These subsequently accelerate neuronal degeneration and finally trigger cognitive impairment (Jack et al., 2013). In this respect, Aβ, tau, and cortical atrophy are primary components of AD pathology (Jack et al., 2016). As a representative value for each pathology, we measured the global extent of tau and Aβ, and the cortical thickness of each subject. In tau PET imaging, we acquired images with GM probability >0.5 and extracted average tau SUVR value per subject in ROIs covering Braak stages (Hoenig et al., 2017). In

this step, we excluded the ROIs in basal ganglia and thalamus due to the off-target effect of THK-5351 (Harada et al., 2016). In Aβ PET imaging, we acquired images with GM probability >0.5 and measured a global amyloid value for combined ROIs (Jack et al., 2010). We calculated the mean cortical thickness among 68 ROIs as a global thickness value per subject. In terms of demographics, age and sex were considered relevant to AD (Li and Singh, 2014; Niccoli and Partridge, 2012) along with apolipoprotein E allele 4 (ApoE ε4), another well-known risk factor for AD (Blacker et al., 1997; Tsai et al., 1994). TIV was used as an estimate of brain reserve and a covariate for cortical thickness (Schofield et al., 1995). Then, we performed multiple linear regression with a dependent variable of cognitive composite score; independent variables of global tau, Aβ deposition and global thickness (AD neuropathology); covariates of age, sex, ApoE ε4 state, and TIV. The resulting beta coefficients of these variables were used to calculate an estimated cognitive composite score. With this assumption, we defined the CR marker as a residual, namely the difference between the actual and estimated cognitive performance, as follows.

$$\text{Cognition}_{estimated} = \beta_0 + \beta_1 \times X_{Tau} + \beta_2 \times X_{A\beta} + \beta_3 \times X_{Cth} + \beta_4 \times X_{Age} + \beta_5 \times X_{Sex} + \beta_6 \times X_{ApoE\ \varepsilon 4} + \beta_7 \times X_{TIV}$$

$$\text{Cognitive reserve (CR)} = \text{Cognition}_{observed} - \text{Cognition}_{estimated}$$

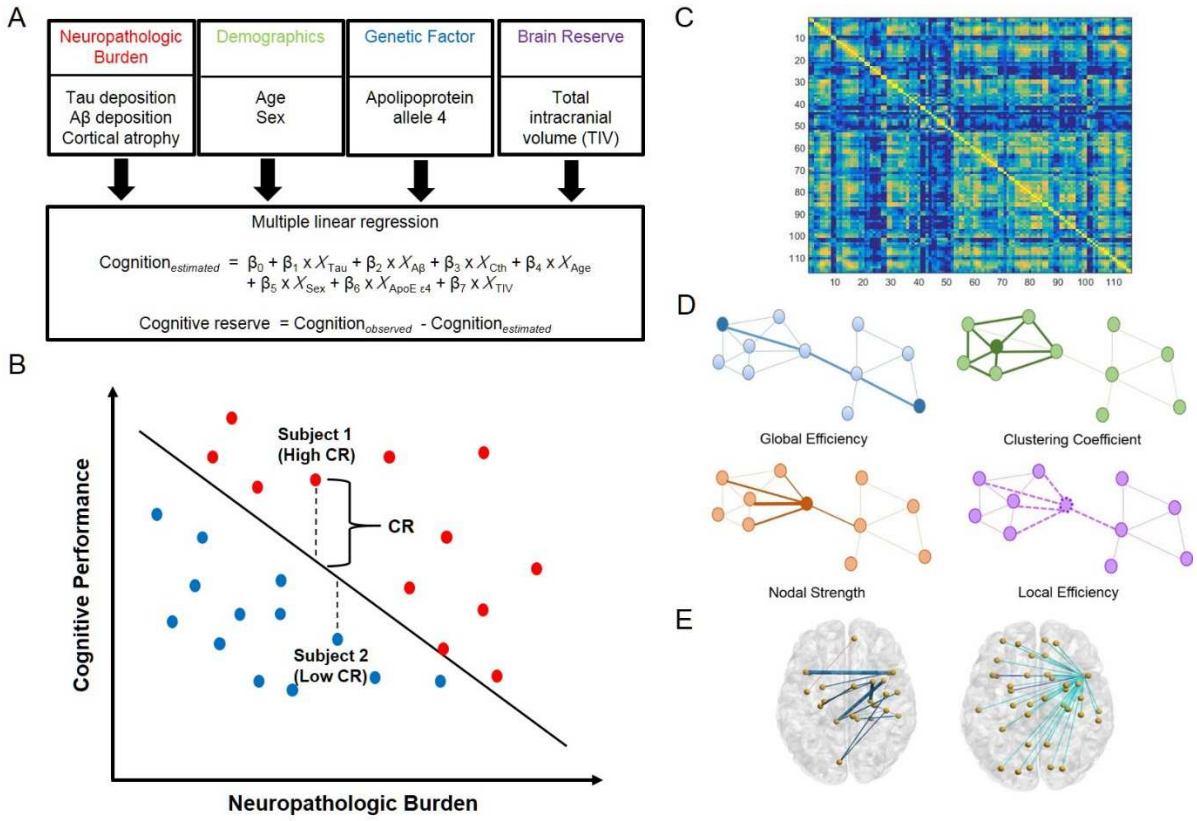

Figure 1. Schematic illustration of our intuitive model for conceptualizing CR. **A:** CR is defined as a residual, namely the difference between actual cognitive performance and estimated performance in our model. $Cognition_{observed:}$ actual cognitive composite score; X_{Tau}: global tau deposition value; $X_{A\beta}$: global Aβ deposition value; X_{Cth}: global cortical thickness value; X_{ApoE} ε_4: Apolipoprotein E ε4; $X_{TIV:}$ total intracranial volume. **B:** X-axis 'Neuropathologic burden' denotes the combination of factors incorporating AD pathology, demographics, a genetic factor and brain reserve. **C:** Weighted positive matrix was applied across a range of sparsities for calculating network properties. **D:** Graph theoretical analysis in correlation with CR (Global efficiency and average clustering coefficient in global level and nodal strength, nodal clustering coefficient and local efficiency in local level) **E:** Regional connectivity analysis in correlation with CR (Functional connectivity and degree based statistics analysis)

2. 6. Validation of the CR marker

To validate the CR marker, we calculated Pearson's correlations between CR marker values and a conventional CR proxy, namely years of education. We also conducted multiple linear regression, using education as the dependent variable, the CR marker as the predictor, and cognitive performance, global cortical thickness, age, sex, and TIV as covariates. In addition, we performed a receiver operating characteristic (ROC) curve analysis in a discrete manner to evaluate how precisely the CR marker classified the high- and low-education groups. These two groups were divided according to the median value of education (12.0 years). Secondly, we also carried out Pearson's correlation between the CR marker and another CR proxy, occupation complexity. DOT scores are composed of three domains, in regards to the complexity of dealing with data (0-6 points), people (0-8 points) and things (0-7 points) (Correa Ribeiro et al., 2013). Lower score indicates higher occupational complexity. We applied a one-tailed significance threshold as we assumed that our CR marker would correlate with DOT ratings in a negative way. We respectively analyzed the correlation between the CR marker and DOT scores in each domain (data, people and things) and subsequently, the total sum of DOT scores.

For the last validation, we investigated whether our CR marker could modify the relationship between brain pathology (tau pathology and cortical thickness) and memory function (memory composite score). To identify the regions that more years of education allow the subjects to tolerate better tau pathology in AD spectrum, we firstly performed voxel wise multiple linear regression of tau PET data with education as independent variable, controlling for age, sex and MMSE among AD spectrum. The resulting *t* statistics map was thresholded at the voxel level at α=0.01 and corrected at the cluster level at α =0.01. After that, we extracted the average tau SUVR within identified regions for each subject. Then we tested the interaction of CR marker X tau SUVR (identified CR-related regions) on memory, controlling for age and sex in AD spectrum. We carried out similar procedures with cortical

thickness data in ROI-wise (68 Desikan-Killiany), adjusting for age, sex, MMSE and TIV among AD spectrum. To find regions that more education allow the patients to cope better with cortical atrophy in AD spectrum, the significance was regarded at FDR-corrected $p < 0.05$. We obtained the average cortical thickness value within significant regions, and calculated atrophy value as a reciprocal of thickness value per subject. Finally, we tested the interaction of CR marker X cortical atrophy within areas on memory, adjusting for age, sex, TIV in AD spectrum.

2. 7. Network construction

We defined the network nodes as the 116 AAL atlas regions, and extracted the average time-series for each ROI from preprocessed fMRI (Tzourio-Mazoyer et al., 2002). AAL atlas is probably the most widely used parcellation method in the field of functional connectome, as it is convenient and labelled according to brain anatomy. As a measure of functional connectivity (FC), Pearson's correlation coefficients were calculated between each pair of ROIs. We only considered the weighted positive matrices in our study. In the graph theory analysis, the matrices were thresholded at various sparsity thresholds (from 0.1 to 0.45 at intervals of 0.01). These ranges were chosen to maintain small-worldness in the network (Tian et al., 2011).

2. 8. Graph theory analysis

We performed graph theoretic analyses at global and local network levels to explore the neural substrates of CR across different levels of granularity. The network metrics were computed using the brain connectivity toolbox (http://www.brain-connectivity-toolbox.net).

Two global network properties were calculated: 1) global efficiency — the average inverse

shortest path length in the network — as a measure of integration in the entire network, and 2) average clustering coefficient — the mean of all nodal clustering values — as a measure of functional segregation across the network. Three additional network properties were assessed at a local level: 1) strength, namely the sum of the weights of links connected to the node; 2) clustering coefficient, namely the fraction of triangles around a node; and 3) local efficiency, which is defined as the average of the inverse shortest path length in the neighborhood of the node (Rubinov and Sporns, 2010).

The nodal strength of node *i* ($S(i)$) is defined as the sum of the connectivity weights of the edges attached to each node *i.*

$$S(i) = \sum_{j \neq i} W_{ij}$$

The clustering coefficient of node *i* ($C(i)$) is computed as:

$$C(i) = \frac{2\, t_i}{k_i\, (k_i - 1)}$$

where k_i is the degree of node *i* and t_i is the number of closed triangles attached to *i*.

The local efficiency of node *i* ($Eloc\ (i)$) is calculated as:

$$Eloc\ (i) = \frac{1}{N_{Gi}\ (N_{Gi} - 1)} \sum_{j,h \in Gi} \frac{1}{l_{jh}}$$

where G_i denotes the subgraph comprising all nodes that are immediate neighbors of the node *i*. l_{jh} is the shortest path length from node *j* to *h*.

Finally, we computed integrated measures of each global or local metric throughout all network sparsity (Marques et al., 2016; Tian et al., 2011). This method can reduce the number of comparisons as well as the complexity of analyses.

$$X_{global}(i) = \sum_{k=10}^{45} X(k \triangle s) \triangle s$$

where $\triangle s$ is the sparsity interval of 0.01; $X(k \triangle s)$ is a global network property (global efficiency and average clustering coefficient) at a sparsity of $k \triangle s$.

$$X_{local}(i) = \sum_{k=10}^{45} X(i, k \triangle s) \triangle s$$

where $X(i, k \triangle s)$ is a local network property (nodal strength, clustering coefficient and local efficiency) at a sparsity of $k \triangle s$.

2. 9. Functional connectivity analysis

We calculated correlations between the CR marker and FC at the edge level. Additionally, we specified one node as a seed, based on the results of local-level analysis, and performed seed to ROI analysis. Finally, to enhance the statistical power of the edge-level analysis, we conducted degree-based statistics analysis (DBS), a novel method for cluster-wise inference. DBS defines a cluster as a set of edges, among which the central node is shared, enabling efficient detection of clusters and center nodes (Yoo et al., 2017). In DBS analysis, an initial cluster-forming threshold was examined at $p < 0.05$, with FWE-corrected $p < 0.05$ used as a cluster-level threshold for significance.

2. 10. Lobar connectivity weight analysis

We further calculated the lobar connectivity weight (LCW) for each pair of lobes in both hemispheres to explore the relationship of the CR marker with lobar level (Ingalhalikar et al.,

2014; Vanicek et al., 2016). We divided the ROIs into seven lobar-areas (frontoinsular, temporal, parietal, occipital lobe, basal ganglia, sensorimotor area, and cerebellum), as a modification of a previous study (Filippi et al., 2017). We defined LCW for each pair of lobes in the two hemispheres (Lx, Ly) as the sum of connectivity weights between region *i* and *j*.

$$LCW\ (Lx, Ly) = \sum_{i \in Lx, j \in Ly} W_{ij}$$

We carried out partial correlation analysis between the CR marker and each LCW, adjusting for MMSE and age. The results are shown in Supplementary Figure 6.

2. 11. Subsequent analysis

Additionally, we repeated the local level analysis in total subjects using Power ROI to check whether the results might be derived from the usage of specific AAL atlas (Power et al., 2011). We used 5 mm- radius 261 ROIs, indexing the name of ROIs by applying the location of center of mass in each ROI into AAL atlas. We excluded 3 ROIs from original 264 ROIs as the value of correlation matrix in these ROIs was extracted as NaN (Not-a-Number). (Center of mass in three ROIs (x, y, z): (-7, -21, 65) / (20, -29, 60) / (29, 1, 4))

We also performed subgroup analysis according to disease status (AD spectrum and normal aging) for CR behavioral pattern would manifest differentially depending on the group. We separately calculated CR in AD spectrum and normal aging and carried out local and edge level analysis.

2. 12. Statistical analysis

Partial correlations were calculated between the CR marker and each graph metric at a

global level, adjusted for MMSE and age. Global properties were considered significant at $p < 0.05$, and corrected for multiple comparisons using family wise error (FWE), which corresponded to $p < 0.025$ (two parameters).

Pearson's correlation coefficients were calculated between the CR marker and graph metrics at local and edge levels. Local metric results were considered significant at $p < 0.05$, and corrected for multiple comparisons using false discovery rate (FDR) or FWE. FWE-corrected $p < 0.05$ was approximately $p < 0.00014$ (i.e., 348 comparisons: 3 properties × number of nodes). Significance was examined at uncorrected $p < 0.001$ in FC analysis. Further seed-to-ROI analyses were considered significant at FDR-corrected $p < 0.05$. We used R studio (R Studio, Boston, MA), SPSS 12 (SPSS, Chicago, IL) and BrainNet viewer (http://www.nitrc.org/projects/bnv/) for visualizations.

3. Results

3. 1. Demographics

Demographics and cognitive performance of the participants are shown in Table 1. There was no difference in the sex ratio among the three groups; however, the age of the AD group was lower than that of the MCI group or normal subjects. In our dataset, fifteen of AD subjects corresponded to early-onset AD. The AD spectrum group had more ApoE ε4 carriers than the normal-aging group. We confirmed the presence of differences among the three groups in global tau, Aβ deposition, and cortical thickness, as well as in MMSE and cognitive composite scores, as expected.

Table 1. Demographics of subjects

	AD	MCI	Normal	*P value* AD vs MCI	*P value* AD vs Normal	*P value* MCI vs Normal
Age	63.2 (11.3)	69.2 (7.2)	68.7 (6.8)	0.031	0.052	0.966
Sex, F (%)	14 (66.7)	23 (71.9)	22 (64.7)	0.686	0.882	0.532
Education	11.6 (4.4)	11.0 (4.3)	10.6 (4.8)	0.906	0.717	0.918
MMSE	19.4 (5.0)	24.3 (3.6)	28.6 (1.2)	<0.001	<0.001	<0.001
ApoE allele 4 (%)	9 (42.9)	17 (53.1)	6 (17.6)	0.465	0.041	0.003
Disease duration (years)	4.6 (3.1)	3.4 (2.7)		0.158		
Tau deposition	1.39 (0.09)	1.32 (0.11)	1.20 (0.10)	0.052	<0.001	<0.001
Amyloid deposition	1.44 (0.15)	1.50 (0.14)	1.10 (0.07)	0.169	<0.001	<0.001
Cortical thickness	2.29 (0.13)	2.39 (0.11)	2.45 (0.12)	0.008	<0.001	0.072
Total intracranial volume	1.35 (0.12)	1.33 (0.13)	1.37 (0.13)	0.836	0.883	0.464
Cognitive composite score	31.51 (11.09)	42.83 (9.52)	61.03 (7.05)	<0.001	<0.001	<0.001
Memory	46.1 (13.3)	61.6 (14.6)	107.9 (15.2)	0.001	<0.001	<0.001
Executive	56.0 (29.8)	75.5 (24.9)	102.3 (17.5)	0.012	<0.001	<0.001
Language	34.1 (13.8)	37.6 (13.4)	50.8 (5.4)	0.501	<0.001	<0.001
Attention	8.6 (2.3)	9.3 (2.6)	11.1 (2.8)	0.663	0.003	0.014
Visuospatial	12.8 (11.9)	30.2 (6.2)	33.0 (4.5)	<0.001	<0.001	0.286
Barthel - ADL	18.8 (4.07)	19.9 (0.39)	20.0 (0.0)	0.130	0.087	0.980

Values are mean (standard deviation) or number (%). Abbreviations: AD= Alzheimer's disease subjects; MCI= Mild cognitive impairment subjects; MMSE = Mini Mental State Examination; Barthel – ADL= Barthel index of Activities of Daily Living; Cognitive composite score indicates the average score of total five domains. *P* values refer to analysis of variance models, followed by post hoc comparisons (Tukey HSD for multiple comparisons).

3. 2. Validation of the CR marker

To validate the model, we assessed the relationship between cognitive performance and each variable via beta values. As expected, the linear regression model showed that the cognitive composite score was negatively related to global tau (β_{tau} = -18.86) and amyloid deposition values ($\beta_{A\beta}$=-32.05). The global composite score showed a positive correlation with global cortical thickness (β_{Cth} = 34.11). The R-squared value of the model was 0.573 (adjusted R^2 = 0.535, F-test p <0.00001). There was no multicollinearity among variables (maximum variance inflation factor (VIF) <1.9). The correlations between cognitive composite score and global values of each brain pathology were shown in Fig. 2.

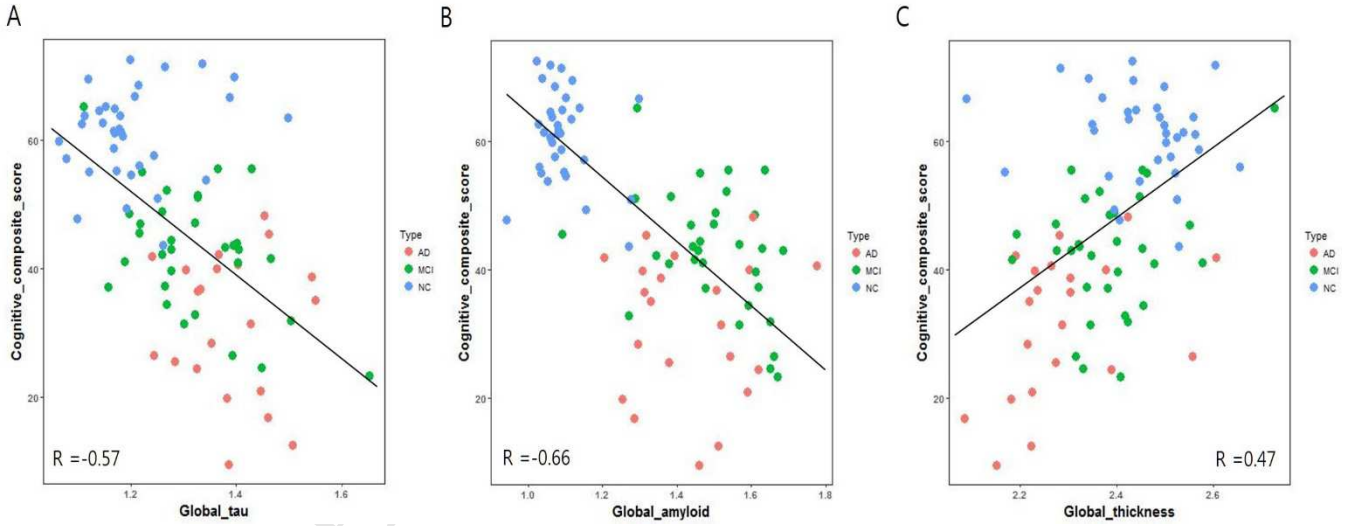

Figure 2. Correlations between cognitive performance and overall AD neuropathology. **A**: Pearson's correlation between cognitive composite score and global tau (R=-0.57). **B**: Pearson's correlation between cognitive composite score and global amyloid (R=-0.66). **C**: Pearson's correlation between cognitive composite score and global cortical thickness (R=0.47).

The CR marker correlated well with years of education (r = 0.44, p <0.00005); subjects with

more years of education had greater CR than individuals with fewer years of education (Fig. 3A). Additionally, the positive association remained between the CR marker and years of education after adjusting cognitive composite score, global cortical thickness, age, sex, and TIV ($t = 2.88$, $p = 0.005$). This result was maintained even after replacing the global thickness measure with global tau and Aβ deposition as covariates ($t = 2.81$, $p = 0.006$). In a discrete ROC curve analysis, the CR marker classified high and low education groups reasonably well (AUC = 0.76, 95% CI = 0.65–0.86; Fig. 3B).

Secondly, the CR marker also correlated with occupation complexity. In our dataset, among the total 87 subjects, 36 participants were housewives and the job of 4 subjects was missing. Therefore, among 47 subjects, our CR marker showed negative correlation with DOT scores in data ($r=-0.26$, $p=0.04$, Fig. 3C) and total sum of DOT scores ($r=-0.34$, $p=0.009$, Fig. 3D), respectively. The CR marker showed no significant correlations with DOT scores in people ($r=-0.21$, $p=0.07$) and things ($r=-0.01$).

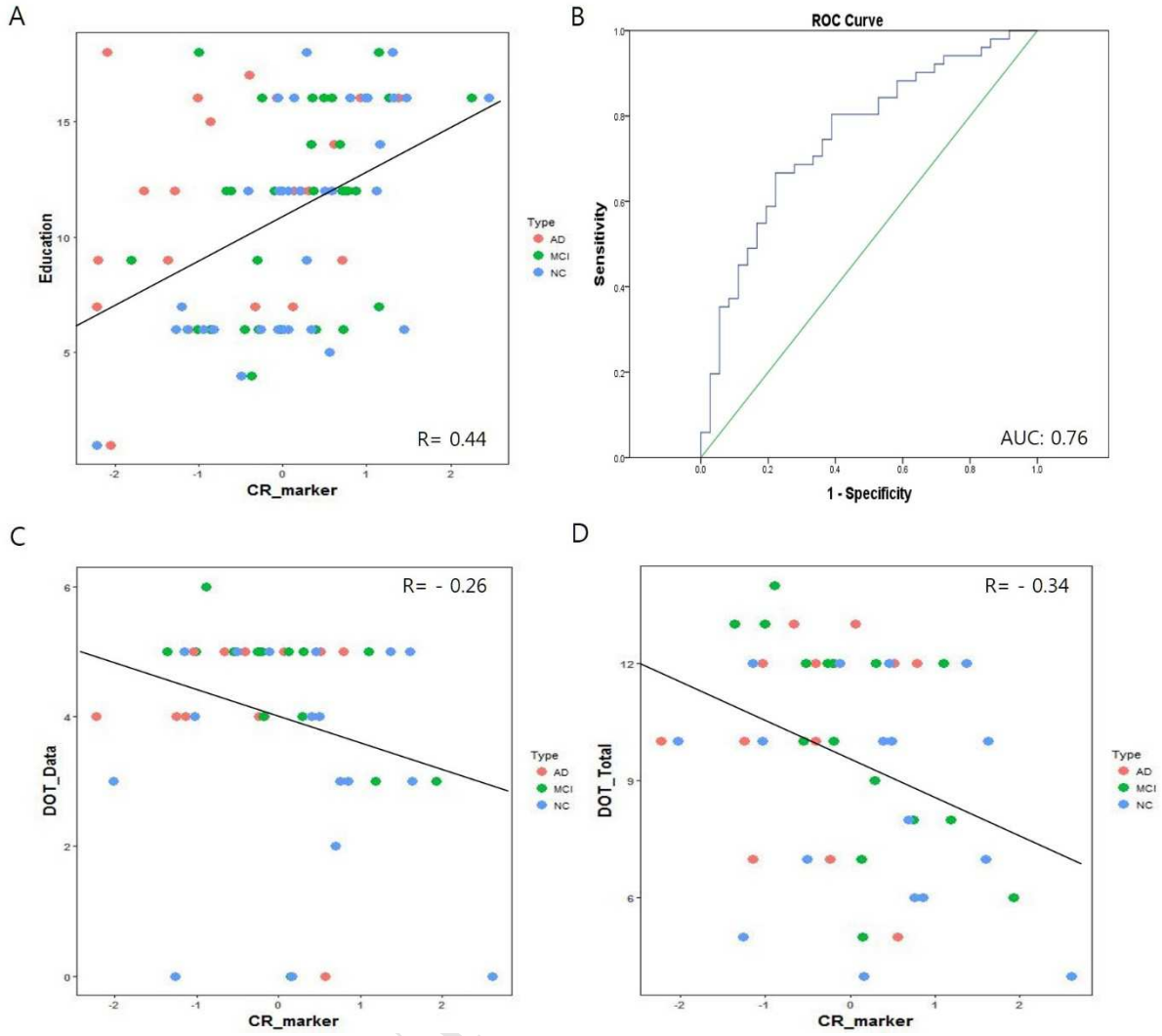

Figure 3. Validation of the CR marker using education and occupation complexity as CR proxies. **A:** Pearson's correlation between the CR marker and education (years). **B:** ROC curve analysis. The CR marker classified high and low educated groups reasonably well (AUC=0.76). **C:** Pearson's correlation between the CR marker and Dictionary Occupational Titles (DOT) scores in data domain. **D:** Pearson's correlation between the CR marker and DOT total scores.

Finally, we assessed whether our CR marker could modulate the association between brain pathology and memory in AD spectrum. In tau pathology, voxel-wise multiple regression

analysis of tau PET data showed that more years of education was associated with higher tau deposition within right temporoparietal regions, controlled for age, sex and MMSE (t=2.29, p=0.02, Fig. 4A). Then, we confirmed that the CR marker modulated the relationship between right temporoparietal tau PET and memory in AD spectrum, controlling for age and sex. Interaction effect of CR marker X right temporoparietal tau-PET on memory function was significant (t-stat=-2.40, p=0.02, Fig. 4B). In cortical thickness, ROI-wise multiple regression analysis found that more education was associated with less cortical thickness (more cortical atrophy) within left inferior temporal gyrus, adjusted for age, sex, MMSE and TIV (Fig. 4C). We defined atrophy value as a reciprocal of thickness value since the atrophy and thickness were in opposite directions. We tested that the CR marker modified the association between left inferior temporal atrophy and memory in AD spectrum, adjusting for age, sex and TIV. We found that the interaction effect of CR marker X left inferior temporal atrophy on memory was significant (t-stat=- 2.76, p=0.008, Fig. 4D). Through this validation, we concluded that our CR marker was validated well as a CR substitute at a reasonable level.

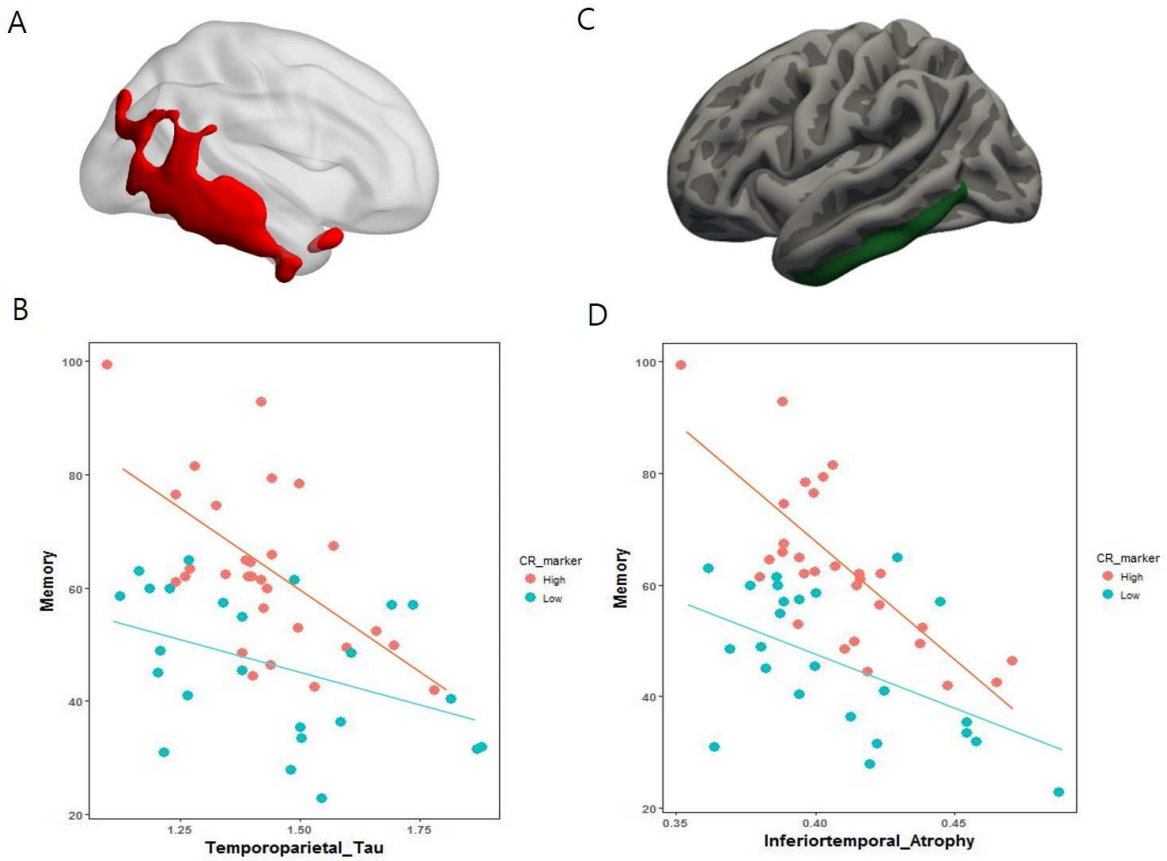

Figure 4. Scatterplot for the interaction of the CR marker X brain pathology (tau and cortical thickness) on memory function in AD spectrum **A:** Tau-related CR showing regions using education as a CR proxy (red color regions, $p < 0.01$ and corrected at the cluster level at $p < 0.01$). **B:** Scatter plot for interaction of CR marker X right temporoparietal tau SUVR on memory score in AD spectrum. For illustration, groups of high and low CR marker (defined via median value) are plotted separately. **C:** Cortical thickness-related CR showing regions using education as a CR proxy (green color areas, FDR $p<0.05$) **D:** Scatter plot for interaction of CR marker X left inferior temporal atrophy value (reciprocal of cortical thickness) on memory score in AD spectrum. For illustration, groups of high and low CR marker (defined via median value) are plotted separately.

3. 3. Associations between the CR marker and network parameters at global and local

network levels

At the global network level, the CR marker was positively correlated with global efficiency (r = 0.25, p = 0.019, t = 2.37) and average clustering coefficient (r = 0.24, p = 0.026, t = 2.27). The latter correlation approached significance after multiple comparison correction (Fig. 5A-B).

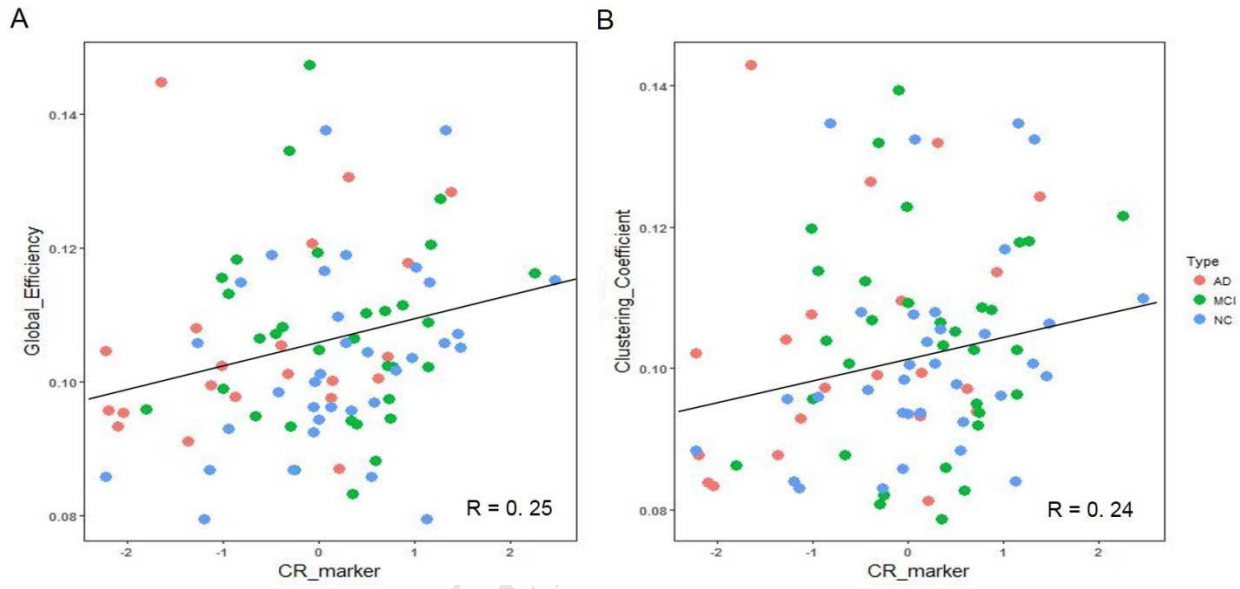

Figure 5. Correlations between the CR marker and global network properties. **A:** Pearson's correlation between the CR marker and global efficiency **B:** Pearson's correlation between the CR marker and average clustering coefficient

At the local network level, the CR marker positively correlated with nodal clustering coefficient and local efficiency in the right middle-temporal pole (Fig. 6A, 6C). This pattern was consistent across all network thresholds. The nodal strength of the right middle-temporal pole also had the highest correlation with the CR marker among all nodes, but did not survive for multiple comparison correction (Fig. 6B). When using derived CR marker only by memory composite score instead of global composite score, we found that the CR marker

still had highest correlation with overall graph measures in the right middle-temporal pole (data not shown). In additional analysis using Power ROI, the right middle-temporal pole maintained the tendency to have highest correlation with the CR marker in graph parameters among all nodes (Supplementary Fig. 1.).

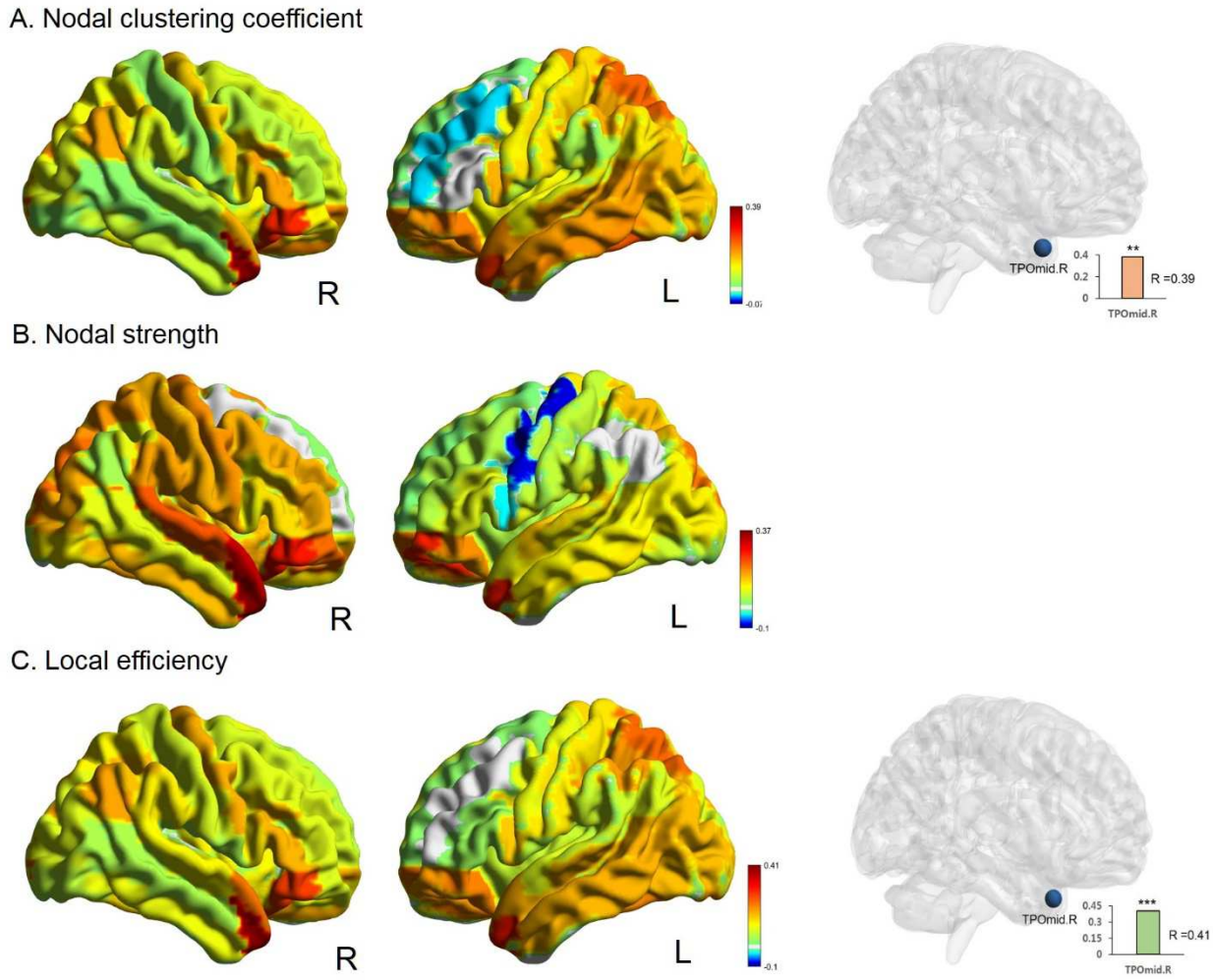

Figure 6. Associations between the CR marker and local graph parameters. **A.** Nodal clustering coefficient **B.** Nodal strength **C.** Local efficiency. Each left and middle figures represent the raw correlation maps between the CR marker and each graph parameter in right (R) and left (L) hemisphere. The scale bar shows the range of correlation values. The right figures in **A** and **C** show the significant ROI (TPOmid.R) correlated with the CR marker in each parameter. In nodal strength (**B**), TPOmid.R had the highest correlation with the CR

marker among all nodes, but did not survive for multiple comparison (R=0.37, uncorrected p<0.0005). **: FDR corrected p<0.05; ***: FWE corrected p<0.05; TPOmid.R: right middle temporal pole

3. 4. Relationship between the CR marker and functional connectivity (FC)

FC with the right middle-temporal pole, which had a positive correlation with the CR marker in the local network analysis, also had the strongest correlation with the CR marker. We further performed seed-to-ROI analysis, using the right middle-temporal pole as a seed. The right middle-temporal pole had significant connectivity with the left amygdala and superior temporal pole, which were positively correlated with the CR marker (correlation between the CR marker and FC with left superior temporal pole: 0.47, with left amygdala: 0.38, $p < 0.05$, with FDR correction). DBS analysis also revealed that one cluster of edges centered on the right middle-temporal pole was significantly associated with the CR marker (initial cluster forming threshold = 0.05, permutation = 5,000, cluster-level threshold = $p < 0.05$, with FWE correction; Fig. 7). All FCs but one showed positive correlations with the CR marker (uncorrected $p < 0.001$, Supplementary Fig. 2). This included FC in sparse cortico-cortical, cortico-subcortical, or cortico-cerebellum networks. One negative FC was connectivity between the right medial frontal gyrus and left precentral gyrus. The lateralization toward the right hemisphere was remarkable among FCs correlated with the CR marker.

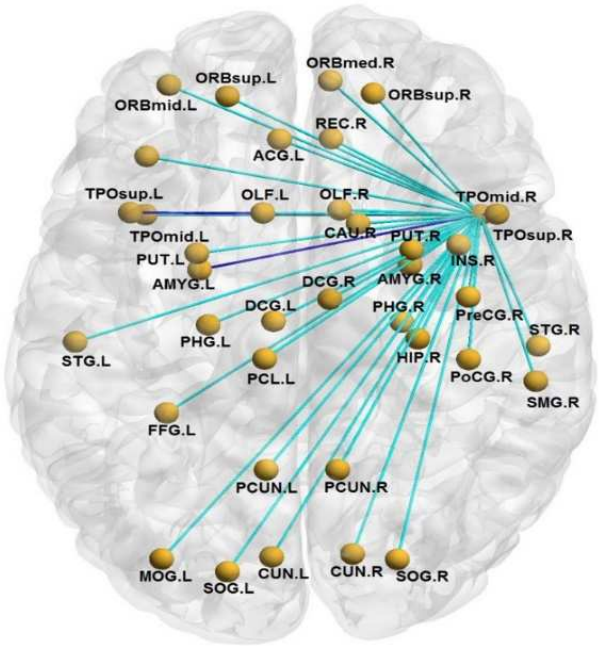

Figure 7. Clusters of edges significantly correlated with the CR marker based on degree-based statistic (DBS). One cluster of edges was found centered on the right middle-temporal pole (icft: 0.05, permutation: 5000, cluster-level threshold: FWE p<0.05). Two dark blue lines denote the FC from right middle-temporal pole to left amygdala or left superior temporal pole in correlation with the CR marker (seed to ROI analysis, FDR p<0.05). The full names of abbreviations are listed in Supplementary Table 1.

3. 5. Subgroup analysis according to disease status

We additionally performed subgroup analysis according to disease status as CR behavioral pattern would manifest differentially depending on the group. In AD spectrum, the CR marker positively correlated with nodal strength in the right middle-temporal pole (Supplementary Fig. 3B, FDR p<0.05). All FCs but one between left amygdala and right pallidum showed positive correlations with the CR marker (Supplementary Fig. 5A). Right middle-temporal

pole as a seed had positive connection with left superior temporal pole in relation to the CR marker (seed to ROI, FDR $p<0.05$). In normal aging, the pattern was different from the disease group. The CR marker in normal aging positively correlated with local efficiency of right precentral gyrus (Supplementary Fig. 4C, FDR $p<0.05$). All FCs except one between left supramarginal gyrus and right inferior occipital gyrus showed positive correlations with the CR marker (Supplementary Fig. 5B). Right precentral gyrus had positive correlations with bilateral cuneus, bilateral supplementary motor area and left postcentral gyrus in relation to the CR marker (seed to ROI, FDR $p<0.05$).

3. 6. Validation of graph measures in right middle-temporal pole as substrates of CR

To confirm that the derived graph theory measures really represent substrates of CR, we first verified whether the CR graph theory measures would be independent of brain pathology. We repeated correlation analysis in global and local level, replacing the CR marker with global tau, amyloid and thickness value respectively. No global network properties were significant for each global value and no significant nodes survived for multiple comparison except for the case of left lingual gyrus in global tau (data not shown).

Second, we tested whether the brain measures of right middle-temporal pole would modulate the relationship between brain pathology (cortical thickness) and cognition (MMSE or memory) in AD spectrum. As a result, nodal clustering coefficient of right middle-temporal pole was revealed to modify the effect of cortical thickness on memory function, controlled for age, sex, TIV and disease stage ($t=-2.08$, $p=0.043$). It showed marginal trends to modulate the effect of thickness on MMSE ($t=-1.99$, $p=0.052$). In case of local efficiency, the interaction effect on memory ($t=-1.92$, $p=0.06$) and MMSE ($t=-1.95$, $p=0.057$) was also marginal.

4. Discussion

In this study, we conceptualized CR based on its original definition, namely the discrepancy between brain pathology and cognitive performance. We validated the CR marker using conventional CR proxies and proved that it modulated the effect of brain pathology on memory. Finally, we explored the neural substrates of CR using network perspective at different network granularities. To accomplish this, we used multimodal neuroimaging including tau, Aβ PET, and structural MRI to quantify the neuropathology, and a global cognitive composite score to quantify cognitive performance. This approach began by estimating the global cognitive composite score based on AD neuropathological burden (tau, Aβ, cortical atrophy), demographics (age and sex), a genetic factor (ApoE ε4), and brain reserve (TIV). Then, we calculated the difference between observed and estimated composite scores as a CR marker for each individual. A greater residual (i.e., higher composite score than expected score) denoted greater CR. Our CR marker was validated using CR proxies. First, the CR marker correlated well with education. Further, the CR marker had a significant linear association with education after adjusting for other covariates. In the ROC curve analysis, the CR marker could classify the more- and less-educated groups reasonably well. Note that discrete analysis is not our primary interest because CR would be distributed in a continuous manner rather than a discrete manner. Secondly, the CR marker correlated with occupation complexity. As we expected, the CR marker negatively correlated with DOT scores in data and total scores of DOT, indicating that the greater CR marker stands for higher occupational complexity. Finally, we examined whether the CR marker modified the effect of brain pathology on memory. We identified CR-showing regions in tau pathology and atrophy with education. Then we examined the interaction of CR marker X brain pathology on memory and proved that the slope of memory decline was more rapid in those with high CR among AD spectrum, representing the phenomenon that

once cognitive decline begins, the rate of decline is more severe in patients with high reserve (Barulli and Stern, 2013). These results support our CR marker as a comprehensive and valid CR surrogate.

Our approach has prospective advantages over existing CR proxies. First, it is intuitive because the parameters of our model are straightforwardly related to the original concept of CR (primarily, neuropathology and cognition). In this approach, we differentiated CR itself from CR proxies, expecting that this would reveal the most relevant properties of CR. Although the use of CR proxies has research value, they have innate shortcomings (Jones et al., 2011). Many variables may be confounding and the mechanisms can be explained using other theories than CR. Therefore, measurement of CR without CR proxies can help to overcome this limitation. Second, we tried to reflect the overall neuropathology of AD by using multimodal neuroimaging methods. Our concept resembles that of a latent variable model, which defines CR as a residual in episodic memory not attributed to brain-related variables or demographics (Marques et al., 2016; Reed et al., 2010; Zahodne et al., 2013) and previous residual model (Habeck et al., 2016). However, our model addresses not only neuronal degeneration (structural atrophy) but also proteinopathies prior to neurodegeneration (Bejanin et al., 2017; Brier et al., 2016; Rolstad et al., 2011). It also encompasses the attention, visuospatial, and language domains, as well as memory and executive function. Third, while typical proxies provide one static value of CR (for example, an individual has only one value for years of education throughout their post-education life), our CR marker is dynamic — it reflects the “present” state of CR. Given that CR depends on current neural activity that is changing continuously according to cognitive exposure or progression of disease, as proposed in the cognitive reserve hypothesis, our CR model fits well with this dynamism.

In this article, we applied graph theory approach as a tool to examine neural substrates associated with CR. By definition, CR is related to the ability to optimize performance

through differential recruitment of brain networks. We especially presumed that CR would represent the concept of efficiency through optimization or differential recruitment. Because graph theory analysis can produce properties of the entire network and respective nodes using mathematical modelling, it could help to identify these features of CR or at least give insight into it.

Our major findings were that the greater CR marker values were related to increased global efficiency and clustering coefficient values. In detail, subjects with higher CR showed higher global efficiency than those with lower CR. Global efficiency is inversely related to the shortest path length in the network and may be interpreted as a measure of the capacity of the system for parallel information transfer and integrated processing (Bullmore and Sporns, 2009). Therefore, it also implies efficient use of limited brain resources, which is one of the essential bases of CR (Stern, 2002). Several studies have shown similar findings regarding CR and functional brain networks (Marques et al., 2016; van den Heuvel et al., 2008). In our study, as well as global efficiency, the correlation between average clustering coefficient and CR approached significance. The average clustering coefficient indicates the functional segregation across the entire network and reflects the ability of the brain to process specialized functions within highly interconnected functional subnetworks (Fornito et al., 2016; Paldino et al., 2017). Although this brain property is known to be associated with cognitive task complexity and AD, its effect on cognition or CR is relatively unknown to date (Supekar et al., 2008; Wen et al., 2015). One study showed that demographic variables, especially education level, were associated with transitivity, which was used as a measure of the global clustering coefficient (Marques et al., 2016). Our result implies that functional segregation as well as integration may contribute to CR, but further studies are required.

Our results suggest that right middle-temporal pole is a potential hub for neural substrates associated with CR. Nodal clustering coefficient and local efficiency in the right middle-temporal pole were correlated significantly with the CR marker. The clustering coefficient

reflects the tendency of nodes to cluster together, and local efficiency measures the extent of integration between the immediate neighbors of a node (Latora and Marchiori, 2001). Local efficiency in particular reflects fault tolerance (a property that enables a system to continue operating properly during certain types of failure) of the system; it indicates the efficiency of communication between the first neighbors of given node when that node is removed (Achard and Bullmore, 2007; Latora and Marchiori, 2003). Consequently, this evidence suggests that the right middle-temporal pole would play a central role when CR manifests at a local network level.

Further, the connectivity of right middle-temporal pole was also significantly correlated with CR. One of the connectivities was with the amygdala, a region associated with cognitive processes and memory (Phelps, 2004; Roozendaal et al., 2009), and the other with the left superior temporal pole (Supplementary Fig. 2); both regions are typically affected by AD pathology. The temporal pole is highly interconnected with the amygdala; therefore, the former is often referred to as a para-limbic region (Blaizot et al., 2010; Olson et al., 2007). The present results highlight the functional relevance of the temporal pole and amygdala in CR, not only in their anatomical relationship. This is supported by the additional DBS analysis, which clearly showed one cluster of edges centered on the right middle-temporal pole was significantly correlated with CR.

Previous studies have recognized that the temporal pole is significantly associated with CR. The temporal pole has been suggested to mediate different cognitive functions such as attention, recognition, emotion, and memory, each of which is presumably related to CR (Damasio et al., 1996; Dolan et al., 2000; Olson et al., 2007; Wong and Gallate, 2012). Subjects with AD spectrum and a high level of education exhibit lower bilateral GM volume in the entorhinal cortex and temporal pole compared to individuals with a low level of education (Serra et al., 2011). In a network flow-based analysis of CR using the white-matter network, the right middle-temporal pole was one of the hub networks that represented a set of

connections affected by education in AD (Wook Yoo et al., 2015). In aspects of bilingualism, another subtype of CR proxy, healthy bilingual individuals showed more preserved temporal-pole cortical thickness or GM volume than monolingual individuals (Abutalebi et al., 2014; Olsen et al., 2015). Previous associations between the temporal pole and CR were based on structural aspects; however, our results revealed that the temporal pole also has important implications regarding CR, from a functional network perspective.

These results seem to be mainly derived from AD spectrum. In subgroup analysis, right middle-temporal pole remained to be associated with the CR marker in AD spectrum. The CR marker significantly correlated with nodal strength in the right middle-temporal pole. Despite not surviving for multiple comparison, right middle-temporal pole showed the greatest correlation with the CR marker in nodal clustering and local efficiency among all nodes. However, the pattern was different in normal aging. The CR marker in normal aging significantly correlated with local efficiency of right precentral gyrus. Right precentral gyrus also showed high correlation with the CR marker in nodal clustering coefficient and nodal strength. In previous study, grey matter density of precentral gyrus was associated with increased secondary network utilization for reserve against age-related change (Steffener and Stern, 2012).

To confirm the graph measures of right middle-temporal pole as neural substrates of CR, we examined whether the measures could mitigate the effect of brain pathology on cognition in AD spectrum. We found that nodal clustering coefficient of right middle-temporal pole modified the effect of cortical thickness on memory, and had marginal effect on the relationship between thickness and MMSE. These results indicate that CR against AD-related pathological changes are represented as neural compensatory mechanism centered on the right middle temporal pole.

Another interesting finding was the right hemispheric lateralization among FCs correlated

with CR as well as LCW analysis (Supplementary Fig. 2 and 6). Several studies have suggested right-hemisphere preferential changes with aging in cognitive tasks (Cherry and Hellige, 1999; Nyberg et al., 2010). The Dallas lifespan brain study revealed that elderly individuals had significantly lower CBF in the right prefrontal region compared to young participants (Lu et al., 2011). Another study found that healthy 50–84 year old adults with ApoEε4 exhibited cerebral metabolic decline over a two-year period, which was particularly marked in the right inferior parietal lobule, and which was associated with a decline in memory performance (Small et al., 2000). A further study found that prefrontal WM volume was reduced in old age. Strikingly, WM volume in the right prefrontal cortex was correlated with cognitive test results (Brickman et al., 2006). Our results are consistent with the idea that the structural and functional integrity of the right prefrontal cortex or parietal lobe is beneficial to CR (Robertson, 2014).

This study has several limitations. First, we recognize that we constructed a relatively simple model of CR. We did not assess interactions among AD pathologies or other neurobiological factors, such as vascular components or white-matter hyper-intensity. In this study, we suggested an intuitive model of CR based on AD pathology and examined its neural substrates using graph theory, rather than producing a model that explains CR perfectly. Second, the AD group was relatively young, and therefore more likely to involve early onset AD; this may introduce the risk of bias. Early onset AD is presumed to be associated with higher CR than late onset AD with similar clinical severity (Bigio et al., 2002; Kim et al., 2005; Marshall et al., 2007). However, in the present study, this issue was not considered in the CR calculation. Third, the number of participants was relatively small; however, the dataset including all tau, amyloid PET, fMRI, and T1 imaging, are still unique and uncommon. Finally, longitudinal studies would be helpful to confirm whether greater CR mitigates cognitive decline or disease progression prospectively.

In conclusion, we proposed an intuitive model to capture CR, using multimodal neuroimaging.

The model incorporates overall neuropathology of AD, demographics, and a genetic factor. Using network perspective, we found that CR is associated with network efficiency for integrated processing, and the right middle-temporal pole could be a center for neural substrates associated with CR in AD spectrum. Our findings will be helpful to identify individuals who are resistant or susceptible to AD pathology. Our approach may be useful for deciding the likely clinical prognosis of patients, and for categorizing patients for drug trials. Subsequently, the middle-temporal pole is a potential target for therapeutic or preventive interventions against AD. Future studies will proceed to investigate whether greater CR mitigates cognitive decline or disease progress.

Acknowledgement

This research was supported by grant HI14C2768 from the Korea Health Technology Research and Development Project through the Korea Health Industry Development Institute, funded by the Ministry of Health & Welfare, Republic of Korea.

Appendix A. Supplementary data

Reference

Abutalebi, J., Canini, M., Della Rosa, P.A., Sheung, L.P., Green, D.W., Weekes, B.S., 2014. Bilingualism protects anterior temporal lobe integrity in aging. Neurobiol Aging 35, 2126-2133.

Achard, S., Bullmore, E., 2007. Efficiency and cost of economical brain functional networks. PLoS Comput Biol 3, e17.

Adam, S., Bonsang, E., Grotz, C., Perelman, S., 2013. Occupational activity and cognitive reserve: implications in terms of prevention of cognitive aging and Alzheimer's disease. Clinical Interventions in Aging 8, 377-390.

Ahn, H.J., Chin, J., Park, A., Lee, B.H., Suh, M.K., Seo, S.W., Na, D.L., 2010. Seoul Neuropsychological

Screening Battery-dementia version (SNSB-D): a useful tool for assessing and monitoring cognitive impairments in dementia patients. J Korean Med Sci 25, 1071-1076.

Barulli, D., Stern, Y., 2013. Efficiency, capacity, compensation, maintenance, plasticity: emerging concepts in cognitive reserve. Trends Cogn Sci 17, 502-509.

Bejanin, A., Schonhaut, D.R., La Joie, R., Kramer, J.H., Baker, S.L., Sosa, N., Ayakta, N., Cantwell, A., Janabi, M., Lauriola, M., O'Neil, J.P., Gorno-Tempini, M.L., Miller, Z.A., Rosen, H.J., Miller, B.L., Jagust, W.J., Rabinovici, G.D., 2017. Tau pathology and neurodegeneration contribute to cognitive impairment in Alzheimer's disease. Brain 140, 3286-3300.

Benton, A.L., Hamsher, K.d., 1989. Multilingual aphasia examination. Iowa City: AJA Associates.

Bigio, E.H., Hynan, L.S., Sontag, E., Satumtira, S., White, C.L., 2002. Synapse loss is greater in presenile than senile onset Alzheimer disease: implications for the cognitive reserve hypothesis. Neuropathology and Applied Neurobiology 28, 218-227.

Blacker, D., Haines, J.L., Rodes, L., Terwedow, H., Go, R.C.P., Harrell, L.E., Perry, R.T., Bassett, S.S., Chase, G., Meyers, D., Albert, M.S., Tanzi, R., 1997. ApoE-4 and age at onset of Alzheimer's disease: The NIMH genetics initiative. Neurology 48, 139-147.

Blaizot, X., Mansilla, F., Insausti, A.M., Constans, J.M., Salinas-Alaman, A., Pro-Sistiaga, P., Mohedano-Moriano, A., Insausti, R., 2010. The human parahippocampal region: I. Temporal pole cytoarchitectonic and MRI correlation. Cereb Cortex 20, 2198-2212.

Braak, H., de Vos, R.A., Jansen, E.N., Bratzke, H., Braak, E., 1998. Neuropathological hallmarks of Alzheimer's and Parkinson's diseases. Prog Brain Res 117, 267-285.

Brickman, A.M., Zimmerman, M.E., Paul, R.H., Grieve, S.M., Tate, D.F., Cohen, R.A., Williams, L.M., Clark, C.R., Gordon, E., 2006. Regional white matter and neuropsychological functioning across the adult lifespan. Biol Psychiatry 60, 444-453.

Brier, M.R., Gordon, B., Friedrichsen, K., McCarthy, J., Stern, A., Christensen, J., Owen, C., Aldea, P., Su, Y., Hassenstab, J., Cairns, N.J., Holtzman, D.M., Fagan, A.M., Morris, J.C., Benzinger, T.L., Ances, B.M., 2016. Tau and Abeta imaging, CSF measures, and cognition in Alzheimer's disease. Sci Transl Med 8, 338ra366.

Bullmore, E., Sporns, O., 2009. Complex brain networks: graph theoretical analysis of structural and functional systems. Nat Rev Neurosci 10, 186-198.

Cherry, B.J., Hellige, J.B., 1999. Hemispheric asymmetries in vigilance and cerebral arousal mechanisms in younger and older adults. Neuropsychology 13, 111-120.

Chiotis, K., Saint-Aubert, L., Savitcheva, I., Jelic, V., Andersen, P., Jonasson, M., Eriksson, J., Lubberink, M., Almkvist, O., Wall, A., Antoni, G., Nordberg, A., 2016. Imaging in-vivo tau pathology in Alzheimer's disease with THK5317 PET in a multimodal paradigm. Eur J Nucl Med Mol Imaging 43, 1686-1699.

Chung, J., Yoo, K., Lee, P., Kim, C.M., Roh, J.H., Park, J.E., Kim, S.J., Seo, S.W., Shin, J.H., Seong, J.K., Jeong, Y., 2017. Normalization of cortical thickness measurements across different T1 magnetic resonance imaging protocols by novel W-Score standardization. Neuroimage 159, 224-235.

Correa Ribeiro, P.C., Lopes, C.S., Lourenco, R.A., 2013. Complexity of lifetime occupation and cognitive performance in old age. Occup Med (Lond) 63, 556-562.

Damasio, H., Grabowski, T.J., Tranel, D., Hichwa, R.D., Damasio, A.R., 1996. A neural basis for lexical retrieval. Nature 380, 499-505.

Desikan, R.S., Segonne, F., Fischl, B., Quinn, B.T., Dickerson, B.C., Blacker, D., Buckner, R.L., Dale, A.M., Maguire, R.P., Hyman, B.T., Albert, M.S., Killiany, R.J., 2006. An automated labeling system for subdividing the human cerebral cortex on MRI scans into gyral based regions of interest. Neuroimage 31, 968-980.

Dolan, R.J., Lane, R., Chua, P., Fletcher, P., 2000. Dissociable temporal lobe activations during emotional episodic memory retrieval. Neuroimage 11, 203-209.

Ewers, M., Insel, P.S., Stern, Y., Weiner, M.W., Alzheimer's Disease Neuroimaging, I., 2013. Cognitive reserve associated with FDG-PET in preclinical Alzheimer disease. Neurology 80, 1194-1201.

Fabrigoule, C., Letenneur, L., Dartigues, J.F., Zarrouk, M., Commenges, D., Barbergergateau, P., 1995. Social and Leisure Activities and Risk of Dementia - a Prospective Longitudinal-Study. Journal of the American Geriatrics Society 43, 485-490.

Filippi, M., Basaia, S., Canu, E., Imperiale, F., Meani, A., Caso, F., Magnani, G., Falautano, M., Comi, G., Falini, A., Agosta, F., 2017. Brain network connectivity differs in early-onset neurodegenerative dementia. Neurology 89, 1764-1772.

Fornito, A., Zalesky, A., Bullmore, E., 2016. Fundamentals of Brain Network Analysis: 1st Edition, San Diego: Academic Press. 268-272.

Habeck, C., Razlighi, Q., Gazes, Y., Barulli, D., Steffener, J., Stern, Y., 2016. Cognitive Reserve and Brain Maintenance: Orthogonal Concepts in Theory and Practice. Cereb Cortex.

Hall, C.B., Derby, C., LeValley, A., Katz, M.J., Verghese, J., Lipton, R.B., 2007. Education delays accelerated decline on a memory test in persons who develop dementia. Neurology 69, 1657-1664.

Harada, R., Okamura, N., Furumoto, S., Furukawa, K., Ishiki, A., Tomita, N., Tago, T., Hiraoka, K., Watanuki, S., Shidahara, M., Miyake, M., Ishikawa, Y., Matsuda, R., Inami, A., Yoshikawa, T., Funaki, Y., Iwata, R., Tashiro, M., Yanai, K., Arai, H., Kudo, Y., 2016. 18F-THK5351: A Novel PET Radiotracer for Imaging Neurofibrillary Pathology in Alzheimer Disease. J Nucl Med 57, 208-214.

Hoenig, M.C., Bischof, G.N., Hammes, J., Faber, J., Fliessbach, K., van Eimeren, T., Drzezga, A., 2017. Tau pathology and cognitive reserve in Alzheimer's disease. Neurobiology of Aging 57, 1-7.

Ingalhalikar, M., Smith, A., Parker, D., Satterthwaite, T.D., Elliott, M.A., Ruparel, K., Hakonarson, H., Gur, R.E., Gur, R.C., Verma, R., 2014. Sex differences in the structural connectome of the human brain. Proc Natl Acad Sci U S A 111, 823-828.

Jack, C.R., Bennett, D.A., Blennow, K., Carrillo, M.C., Feldman, H.H., Frisoni, G.B., Hampel, H., Jagust, W.J., Johnson, K.A., Knopman, D.S., Petersen, R.C., Scheltens, P., Sperling, R.A., Dubois, B., 2016. A/T/N: An unbiased descriptive classification scheme for Alzheimer disease biomarkers. Neurology 87, 539-547.

Jack, C.R., Jr., Knopman, D.S., Jagust, W.J., Petersen, R.C., Weiner, M.W., Aisen, P.S., Shaw, L.M., Vemuri, P., Wiste, H.J., Weigand, S.D., Lesnick, T.G., Pankratz, V.S., Donohue, M.C., Trojanowski, J.Q., 2013. Tracking pathophysiological processes in Alzheimer's disease: an updated hypothetical model of dynamic biomarkers. Lancet Neurol 12, 207-216.

Jack, C.R., Jr., Wiste, H.J., Vemuri, P., Weigand, S.D., Senjem, M.L., Zeng, G., Bernstein, M.A., Gunter, J.L., Pankratz, V.S., Aisen, P.S., Weiner, M.W., Petersen, R.C., Shaw, L.M., Trojanowski, J.Q., Knopman, D.S., Alzheimer's Disease Neuroimaging, I., 2010. Brain beta-amyloid measures and magnetic resonance imaging atrophy both predict time-to-progression from mild cognitive impairment to Alzheimer's disease. Brain 133, 3336-3348.

Jahng., S., Na., D.L., Kang., Y., 2015. Constructing a Composite Score for the Seoul Neuropsychological Screening Battery-Core. Dement Neurocognitive Disord 14, 137-142.

Jones, R.N., Manly, J., Glymour, M.M., Rentz, D.M., Jefferson, A.L., Stern, Y., 2011. Conceptual and measurement challenges in research on cognitive reserve. J Int Neuropsychol Soc 17, 593-601.

Joshi, A., Koeppe, R.A., Fessler, J.A., 2009. Reducing between scanner differences in multi-center PET studies. Neuroimage 46, 154-159.

Kang, Y.W., Na, D.L., 2003. Seoul Neuropsychological Screening Battery. Human Brain Research & Consulting Co. Seoul.

Katzman, R., Terry, R., Deteresa, R., Brown, T., Davies, P., Fuld, P., Xiong, R.B., Peck, A., 1988. Clinical, Pathological, and Neurochemical Changes in Dementia - a Subgroup with Preserved Mental Status and Numerous Neocortical Plaques. Annals of Neurology 23, 138-144.

Kemppainen, N.M., Aalto, S., Karrasch, M., Nagren, K., Savisto, N., Oikonen, V., Viitanen, M., Parkkola, R., Rinne, J.O., 2008. Cognitive reserve hypothesis: Pittsburgh Compound B and fluorodeoxyglucose positron emission tomography in relation to education in mild Alzheimer's disease. Ann Neurol 63, 112-118.

Kim, E.J., Cho, S.S., Jeong, Y., Park, K.C., Kang, S.J., Kang, E., Kim, S.E., Lee, K.H., Na, D.L., 2005. Glucose metabolism in early onset versus late onset Alzheimer's disease: an SPM analysis of 120 patients. Brain 128, 1790-1801.

Kim, H., Na, D.L., 1999. Normative data on the Korean version of the Boston Naming Test. J Clin Exp Neuropsychol 21, 127-133.

Labor., U.S.D.o., 1977. Dictionary of occupational titles (4th Ed.). Goverment Printing Office, Washington, D.C.

Langer, N., Pedroni, A., Gianotti, L.R., Hanggi, J., Knoch, D., Jancke, L., 2012. Functional brain network efficiency predicts intelligence. Hum Brain Mapp 33, 1393-1406.

Latora, V., Marchiori, M., 2001. Efficient behavior of small-world networks. Physical Review Letters 87, 198701.

Latora, V., Marchiori, M., 2003. Economic small-world behavior in weighted networks. European Physical Journal B 32, 249-263.

Lezak, M.D., 1995. Neuropsychological Assessment. Oxford University Press, 545.

Li, R.N., Singh, M., 2014. Sex differences in cognitive impairment and Alzheimer's disease. Frontiers in Neuroendocrinology 35, 385-403.

Liu, Y., Liang, M., Zhou, Y., He, Y., Hao, Y., Song, M., Yu, C., Liu, H., Liu, Z., Jiang, T., 2008. Disrupted small-world networks in schizophrenia. Brain 131, 945-961.

Liu, Y.W., Julkunen, V., Paajanen, T., Westman, E., Wahlund, L.O., Aitken, A., Sobow, T., Mecocci, P., Tsolaki, M., Vellas, B., Muehlboeck, S., Spenger, C., Lovestone, S., Simmons, A., Soininen, H., Consortium, A., 2012. Education increases reserve against Alzheimer's disease-evidence from structural MRI analysis. Neuroradiology 54, 929-938.

Lu, H., Xu, F., Rodrigue, K.M., Kennedy, K.M., Cheng, Y., Flicker, B., Hebrank, A.C., Uh, J., Park, D.C., 2011. Alterations in cerebral metabolic rate and blood supply across the adult lifespan. Cereb Cortex 21, 1426-1434.

Marques, P., Moreira, P., Magalhaes, R., Costa, P., Santos, N., Zihl, J., Soares, J., Sousa, N., 2016. The functional connectome of cognitive reserve. Hum Brain Mapp 37, 3310-3322.

Marshall, G.A., Fairbanks, L.A., Tekin, S., Vinters, H.V., Cummings, J.L., 2007. Early-onset Alzheimer's disease is associated with greater pathologic burden. Journal of Geriatric Psychiatry and Neurology 20, 29-33.

McKhann, G.M., Knopman, D.S., Chertkow, H., Hyman, B.T., Jack, C.R., Jr., Kawas, C.H., Klunk, W.E., Koroshetz, W.J., Manly, J.J., Mayeux, R., Mohs, R.C., Morris, J.C., Rossor, M.N., Scheltens, P., Carrillo, M.C., Thies, B., Weintraub, S., Phelps, C.H., 2011. The diagnosis of dementia due to Alzheimer's disease: recommendations from the National Institute on Aging-Alzheimer's Association workgroups on diagnostic guidelines for Alzheimer's disease. Alzheimers Dement 7, 263-269.

Meng, X.F., D'Arcy, C., 2012. Education and Dementia in the Context of the Cognitive Reserve Hypothesis: A Systematic Review with Meta-Analyses and Qualitative Analyses. PLoS One 7.

Meunier, D., Lambiotte, R., Fornito, A., Ersche, K.D., Bullmore, E.T., 2009. Hierarchical modularity in human brain functional networks. Front Neuroinform 3, 37.

Meyers, J.E., Meyers, K.R., 1995. Rey Complex Figure Test and recognition trial: Professional manual. Lutz, FL: Psychological Assessment Resources.

Mueller, S., Wang, D., Fox, M.D., Yeo, B.T., Sepulcre, J., Sabuncu, M.R., Shafee, R., Lu, J., Liu, H., 2013. Individual variability in functional connectivity architecture of the human brain. Neuron 77, 586-595.

Niccoli, T., Partridge, L., 2012. Ageing as a Risk Factor for Disease. Current Biology 22, R741-R752.

Nyberg, L., Salami, A., Andersson, M., Eriksson, J., Kalpouzos, G., Kauppi, K., Lind, J., Pudas, S., Persson, J., Nilsson, L.G., 2010. Longitudinal evidence for diminished frontal cortex function in aging. Proceedings of the National Academy of Sciences of the United States of America 107, 22682-22686.

Olsen, R.K., Pangelinan, M.M., Bogulski, C., Chakravarty, M.M., Luk, G., Grady, C.L., Bialystok, E., 2015. The effect of lifelong bilingualism on regional grey and white matter volume. Brain Res 1612, 128-139.

Olson, I.R., Plotzker, A., Ezzyat, Y., 2007. The Enigmatic temporal pole: a review of findings on social and emotional processing. Brain 130, 1718-1731.

Paldino, M.J., Zhang, W., Chu, Z.D., Golriz, F., 2017. Metrics of brain network architecture capture the impact of disease in children with epilepsy. Neuroimage Clin 13, 201-208.

Petersen, R.C., Smith, G.E., Waring, S.C., Ivnik, R.J., Tangalos, E.G., Kokmen, E., 1999. Mild cognitive impairment: clinical characterization and outcome. Arch Neurol 56, 303-308.

Phelps, E.A., 2004. Human emotion and memory: interactions of the amygdala and hippocampal complex. Curr Opin Neurobiol 14, 198-202.

Power, J.D., Cohen, A.L., Nelson, S.M., Wig, G.S., Barnes, K.A., Church, J.A., Vogel, A.C., Laumann, T.O., Miezin, F.M., Schlaggar, B.L., Petersen, S.E., 2011. Functional network organization of the human brain. Neuron 72, 665-678.

Reed, B.R., Mungas, D., Farias, S.T., Harvey, D., Beckett, L., Widaman, K., Hinton, L., DeCarli, C., 2010. Measuring cognitive reserve based on the decomposition of episodic memory variance. Brain 133, 2196-2209.

Richards, M., Sacker, A., 2003. Lifetime antecedents of cognitive reserve. Journal of Clinical and Experimental Neuropsychology 25, 614-624.

Robertson, I.H., 2014. Right hemisphere role in cognitive reserve. Neurobiol Aging 35, 1375-1385.

Rolstad, S., Berg, A.I., Bjerke, M., Blennow, K., Johansson, B., Zetterberg, H., Wallin, A., 2011. Amyloid-beta(4)(2) is associated with cognitive impairment in healthy elderly and subjective cognitive impairment. J Alzheimers Dis 26, 135-142.

Roozendaal, B., McEwen, B.S., Chattarji, S., 2009. Stress, memory and the amygdala. Nat Rev Neurosci 10, 423-433.

Rubinov, M., Sporns, O., 2010. Complex network measures of brain connectivity: uses and interpretations. Neuroimage 52, 1059-1069.

Sabri, O., Seibyl, J., Rowe, C., Barthel, H., 2015. Beta-amyloid imaging with florbetaben. Clin Transl Imaging 3, 13-26.

Scarmeas, N., Levy, G., Tang, M.X., Manly, J., Stern, Y., 2001. Influence of leisure activity on the incidence of Alzheimer's disease. Neurology 57, 2236-2242.

Schofield, P.W., Mosesson, R.E., Stern, Y., Mayeux, R., 1995. The Age at Onset of Alzheimers-Disease and an Intracranial Area Measurement - a Relationship. Archives of Neurology 52, 95-98.

Serra, L., Cercignani, M., Petrosini, L., Basile, B., Perri, R., Fadda, L., Spano, B., Marra, C., Giubilei, F., Carlesimo, G.A., Caltagirone, C., Bozzali, M., 2011. Neuroanatomical Correlates of Cognitive Reserve in Alzheimer Disease. Rejuvenation Research 14, 143-151.

Serrano-Pozo, A., Frosch, M.P., Masliah, E., Hyman, B.T., 2011. Neuropathological Alterations in Alzheimer Disease. Cold Spring Harbor Perspectives in Medicine 1.

Small, G.W., Ercoli, L.M., Silverman, D.H., Huang, S.C., Komo, S., Bookheimer, S.Y., Lavretsky, H., Miller, K., Siddarth, P., Rasgon, N.L., Mazziotta, J.C., Saxena, S., Wu, H.M., Mega, M.S., Cummings, J.L., Saunders, A.M., Pericak-Vance, M.A., Roses, A.D., Barrio, J.R., Phelps, M.E., 2000. Cerebral

metabolic and cognitive decline in persons at genetic risk for Alzheimer's disease. Proc Natl Acad Sci U S A 97, 6037-6042.

Steffener, J., Stern, Y., 2012. Exploring the neural basis of cognitive reserve in aging. Biochim Biophys Acta 1822, 467-473.

Stern, Y., 2002. What is cognitive reserve? Theory and research application of the reserve concept. Journal of the International Neuropsychological Society 8, 448-460.

Stern, Y., 2012. Cognitive reserve in ageing and Alzheimer's disease. Lancet Neurology 11, 1006-1012.

Stern, Y., Alexander, G.E., Prohovnik, I., Mayeux, R., 1992. Inverse relationship between education and parietotemporal perfusion deficit in Alzheimer's disease. Ann Neurol 32, 371-375.

Stern, Y., Habeck, C., Moeller, J., Scarmeas, N., Anderson, K.E., Hilton, H.J., Flynn, J., Sackeim, H., van Heertum, R., 2005. Brain networks associated with cognitive reserve in healthy young and old adults. Cerebral Cortex 15, 394-402.

Supekar, K., Menon, V., Rubin, D., Musen, M., Greicius, M.D., 2008. Network analysis of intrinsic functional brain connectivity in Alzheimer's disease. PLoS Comput Biol 4, e1000100.

Tian, L., Wang, J., Yan, C., He, Y., 2011. Hemisphere- and gender-related differences in small-world brain networks: a resting-state functional MRI study. Neuroimage 54, 191-202.

Tsai, M.S., Tangalos, E.G., Petersen, R.C., Smith, G.E., Schaid, D.J., Kokmen, E., Ivnik, R.J., Thibodeau, S.N., 1994. Apolipoprotein-E - Risk Factor for Alzheimer-Disease. American Journal of Human Genetics 54, 643-649.

Tzourio-Mazoyer, N., Landeau, B., Papathanassiou, D., Crivello, F., Etard, O., Delcroix, N., Mazoyer, B., Joliot, M., 2002. Automated anatomical labeling of activations in SPM using a macroscopic anatomical parcellation of the MNI MRI single-subject brain. Neuroimage 15, 273-289.

van den Heuvel, M.P., Sporns, O., 2013. Network hubs in the human brain. Trends Cogn Sci 17, 683-696.

van den Heuvel, M.P., Stam, C.J., Boersma, M., Hulshoff Pol, H.E., 2008. Small-world and scale-free organization of voxel-based resting-state functional connectivity in the human brain. Neuroimage 43, 528-539.

van Loenhoud, A.C., Wink, A.M., Groot, C., Verfaillie, S.C.J., Twisk, J., Barkhof, F., van Berckel, B., Scheltens, P., van der Flier, W.M., Ossenkoppele, R., 2017. A neuroimaging approach to capture cognitive reserve: Application to Alzheimer's disease. Hum Brain Mapp 38, 4703-4715.

Vanicek, T., Hahn, A., Traub-Weidinger, T., Hilger, E., Spies, M., Wadsak, W., Lanzenberger, R., Pataraia, E., Asenbaum-Nan, S., 2016. Insights into Intrinsic Brain Networks based on Graph Theory and PET in right- compared to left-sided Temporal Lobe Epilepsy. Scientific Reports 6.

Watts, D.J., Strogatz, S.H., 1998. Collective dynamics of 'small-world' networks. Nature 393, 440-442.

Wen, X., Zhang, D., Liang, B., Zhang, R., Wang, Z., Wang, J., Liu, M., Huang, R., 2015. Reconfiguration of the Brain Functional Network Associated with Visual Task Demands. PLoS One 10, e0132518.

Wong, C., Gallate, J., 2012. The function of the anterior temporal lobe: a review of the empirical evidence. Brain Res 1449, 94-116.

Wook Yoo, S., Han, C.E., Shin, J.S., Won Seo, S., Na, D.L., Kaiser, M., Jeong, Y., Seong, J.K., 2015. A Network Flow-based Analysis of Cognitive Reserve in Normal Ageing and Alzheimer's Disease. Sci Rep 5, 10057.

Yoo, K., Lee, P., Chung, M.K., Sohn, W.S., Chung, S.J., Na, D.L., Ju, D., Jeong, Y., 2017. Degree-based statistic and center persistency for brain connectivity analysis. Hum Brain Mapp 38, 165-181.

Zahodne, L.B., Manly, J.J., Brickman, A.M., Siedlecki, K.L., Decarli, C., Stern, Y., 2013. Quantifying cognitive reserve in older adults by decomposing episodic memory variance: replication and extension. J Int Neuropsychol Soc 19, 854-862.

Supplementary information

Supplementary Table 1. Network nodes in the AAL template

AAL regions	Abbreviations	AAL regions	Abbreviations
Amygdala (left)	AMYG.L	Inferior occipital gyrus (right)	IOG.R
Amygdala (right)	AMYG.R	Middle occipital gyrus (left)	MOG.L
Angular gyrus (left)	ANG.L	Middle occipital gyrus (right)	MOG.R
Angular gyrus (right)	ANG.R	Superior occipital gyrus (left)	SOG.L
Calcarine fissure and surrounding cortex (left)	CAL.L	Superior occipital gyrus (right)	SOG.R
Calcarine fissure and surrounding cortex (right)	CAL.R	Olfactory cortex (left)	OLF.L
Caudate nucleus (left)	CAU.L	Olfactory cortex (right)	OLF.R
Caudate nucleus (right)	CAU.R	Lenticular nucleus, pallidum (left)	PAL.L
Anterior cingulate and paracingulate gyri (left)	ACG.L	Lenticular nucleus, pallidum (right)	PAL.R
Anterior cingulate and paracingulate gyri (right)	ACG.R	Paracentral lobule (left)	PCL.L
Median cingulate and paracingulate gyri (left)	DCG.L	Paracentral lobule (right)	PCL.R

Median cingulate and paracingulate gyri (right)	DCG.R	Parahippocampal gyrus (left)	PHG.L
Posterior cingulate gyrus (left)	PCG.L	Parahippocampal gyrus (right)	PHG.R
Posterior cingulate gyrus (right)	PCG.R	Inferior parietal, but supra-marginal and angular gyri (left)	IPL.L
Cuneus (left)	CUN.L	Inferior parietal, but supra-marginal and angular gyri (right)	IPL.R
Cuneus (right)	CUN.R	Superior parietal gyrus (left)	SPG.L
Inferior frontal gyrus, opercular part (left)	IFGoperc.L	Superior parietal gyrus (right)	SPG.R
Inferior frontal gyrus, opercular part (right)	IFGoperc.R	Postcentral gyrus (left)	PoCG.L
Inferior frontal gyrus, orbital part (left)	ORBinf.L	Postcentral gyrus (right)	PoCG.R
Inferior frontal gyrus, orbital part (right)	ORBinf.R	Precentral gyrus (left)	PreCG.L
Inferior frontal gyrus, triangular part (left)	IFGtriang.L	Precentral gyrus (right)	PreCG.R
Inferior frontal gyrus, triangular part (right)	IFGtriang.R	Precuneus (left)	PCUN.L
Superior frontal gyrus, medial orbital (left)	ORBmed.L	Precuneus (right)	PCUN.R
Superior frontal gyrus, medial orbital (right)	ORBmed.R	Lenticular nucleus, putamen (left)	PUT.L
Middle frontal gyrus (left)	MFG.L	Lenticular nucleus, putamen (right)	PUT.R
Middle frontal gyrus, orbital part (left)	ORBmid.L	Gyrus rectus (left)	REC.L
Middle frontal gyrus, orbital part (right)	ORBmid.R	Gyrus rectus (right)	REC.R
Middle frontal gyrus (right)	MFG.R	Rolandic operculum (left)	ROL.L
Superior frontal gyrus, dorsolateral (left)	SFGdor.L	Rolandic operculum (right)	ROL.R
Superior frontal gyrus, medial (left)	SFGmed.L	Supplementary motor area (left)	SMA.L

Superior frontal gyrus, medial (right)	SFGmed.R	Supplementary motor area (right)	SMA.R
Superior frontal gyrus, orbital part (left)	ORBsup.L	Supramarginal gyrus (left)	SMG.L
Superior frontal gyrus, orbital part (right)	ORBsup.R	Supramarginal gyrus (right)	SMG.R
Superior frontal gyrus, dorsolateral (right)	SFGdor.R	Inferior temporal gyrus (left)	ITG.L
Fusiform gyrus (left)	FFG.L	Inferior temporal gyrus (right)	ITG.R
Fusiform gyrus (right)	FFG.R	Middle temporal gyrus (left)	MTG.L
Heschl gyrus (left)	HES.L	Middle temporal gyrus (right)	MTG.R
Heschl gyrus (right)	HES.R	Temporal pole: middle temporal gyrus (left)	TPOmid.L
Hippocampus (left)	HIP.L	Temporal pole: middle temporal gyrus (right)	TPOmid.R
Hippocampus (right)	HIP.R	Temporal pole: superior temporal gyrus (left)	TPOsup.L
Insula (left)	INS.L	Temporal pole: superior temporal gyrus (right)	TPOsup.R
Insula (right)	INS.R	Superior temporal gyrus (left)	STG.L
Lingual gyrus (left)	LING.L	Superior temporal gyrus (right)	STG.R
Lingual gyrus (right)	LING.R	Thalamus (left)	THA.L
Inferior occipital gyrus (left)	IOG.L	Thalamus (right)	THA.R
Cerebellum_3 (left)	CRBL3.L	Cerebellum_10 (right)	CRBL10.R
Cerebellum_3 (right)	CRBL3.R	Cerebellum_Crus1 (left)	CRBLCrus1.L
Cerebellum_4_5 (left)	CRBL4_5.L	Cerebellum_Crus1 (right)	CRBLCrus1.R
Cerebellum_4_5 (right)	CRBL4_5.R	Cerebellum_Crus2 (left)	CRBLCrus2.L
Cerebellum_6 (left)	CRBL6.L	Cerebellum_Crus2 (right)	CRBLCrus2.R
Cerebellum_6 (right)	CRBL6.R	Vermis_1_2	Vermis1_2
Cerebellum_7 (left)	CRBL7.L	Vermis_3	Vermis3
Cerebellum_7 (right)	CRBL7.R	Vermis_4_5	Vermis4_5

Cerebellum_8 (left)	CRBL8.L	Vermis_6	Vermis6
Cerebellum_8 (right)	CRBL8.R	Vermis_7	Vermis7
Cerebellum_9 (left)	CRBL9.L	Vermis_8	Vermis8
Cerebellum_9 (right)	CRBL9.R	Vermis_9	Vermis9
Cerebellum_10 (left)	CRBL10.L	Vermis_10	Vermis10

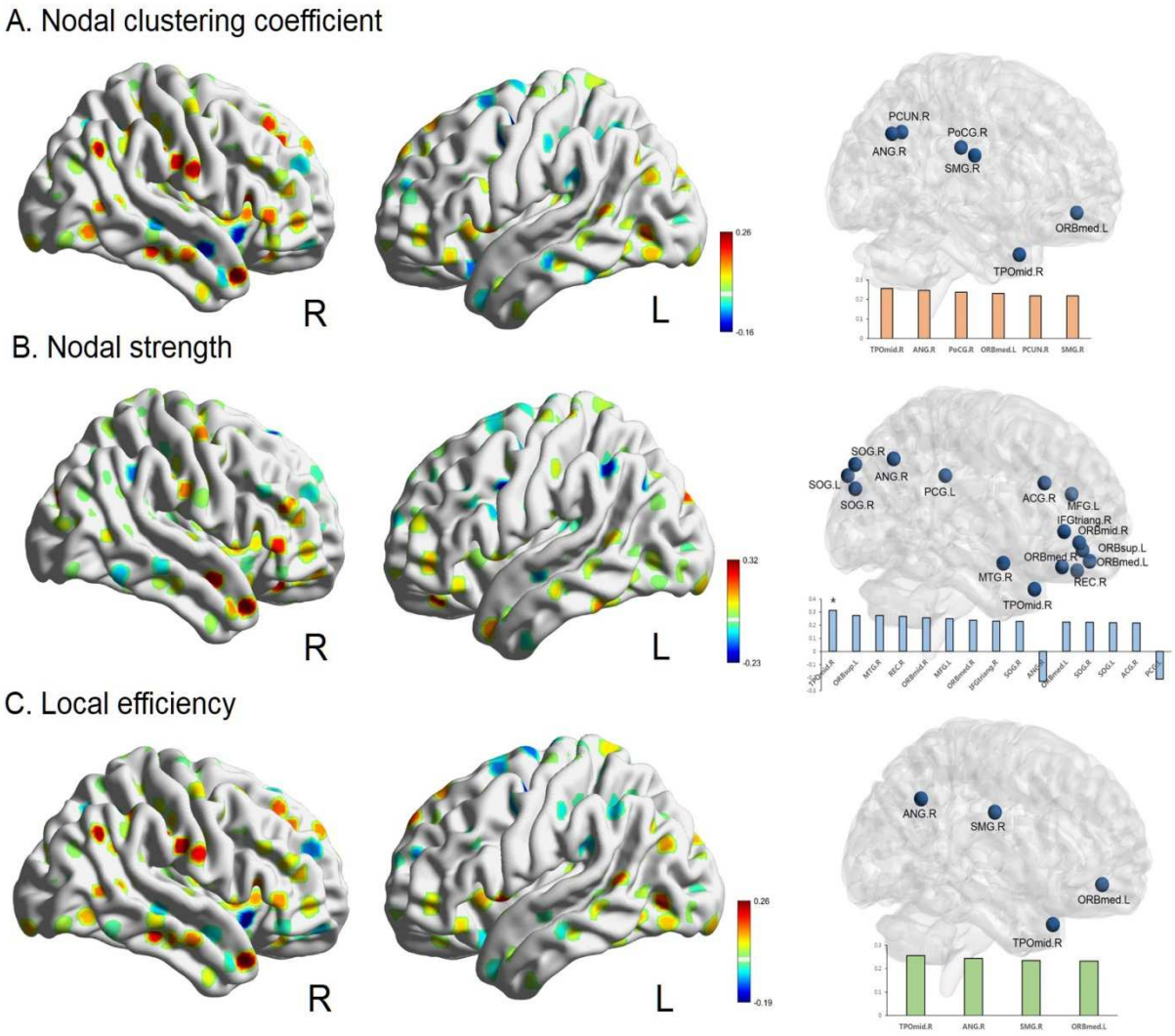

Supplementary Figure 1. Associations between the CR marker and local graph parameters using Power ROI. **A.** Nodal clustering coefficient **B.** Nodal strength **C.** Local efficiency. Each

left and middle figures represent the raw correlation maps between the CR marker and each graph parameter in right (R) and left (L) hemisphere. The scale bar shows the range of correlation values. Each right figure shows the ROIs correlated with the CR marker in each parameter. Although the aspect of correlation was different from using AAL atlas, right middle-temporal pole (TPOmid.R / coordinate of center of mass: (46, 16, -30)) maintained the tendency to have greatest correlation with the CR marker in graph parameters among all nodes. *: uncorrected p<0.005; without any indication: uncorrected p<0.05. The full names of abbreviations in significant ROIs are listed in Supplementary Table 1.

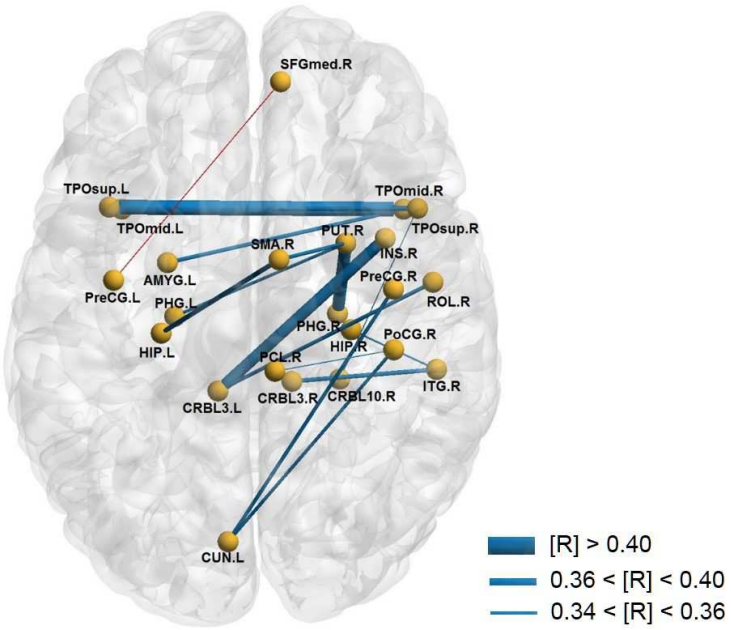

Supplementary Figure 2. The functional connectivity (FC) showing significant correlation with the CR marker (uncorrected p<0.001). Edges of positive correlation are presented in blue and one negative edge is red. The thickness of edge indicates correlation coefficient between each FC and the CR marker (R). The full names of abbreviations are listed in

Supplementary Table 1.

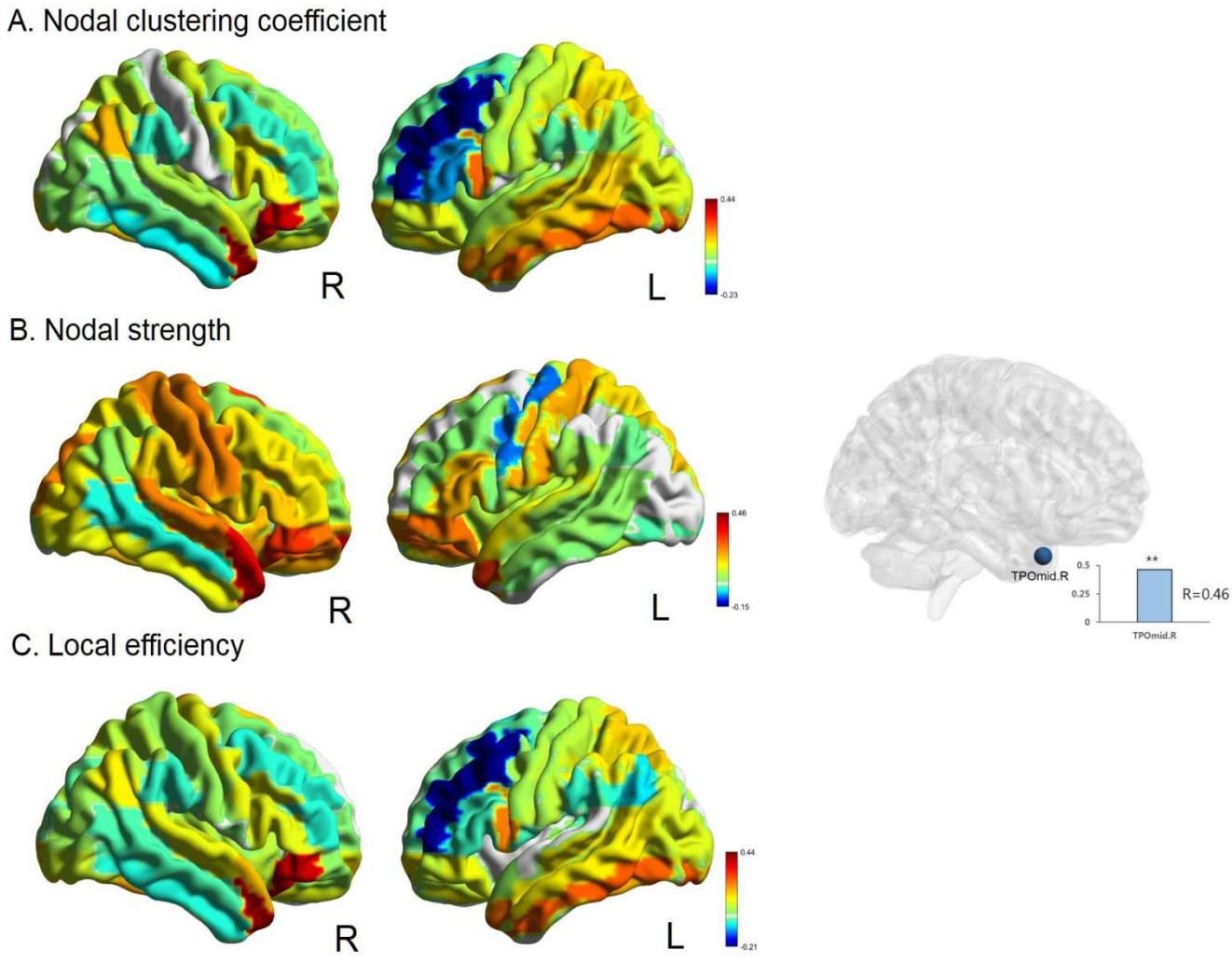

Supplementary Figure 3. Associations between the CR marker and local graph parameters

in AD spectrum. **A.** Nodal clustering coefficient **B.** Nodal strength **C.** Local efficiency. Each left and middle figures represent the raw correlation maps between the CR marker and each graph parameter in right (R) and left (L) hemisphere. The scale bar shows the range of correlation values. The right figure in **B** shows the significant ROI (TPOmid.R) correlated with the CR marker in nodal strength. In nodal clustering coefficient (**A**) and local efficiency (**C**), TPOmid.R had the highest correlation with the CR marker among all nodes, but did not survive for multiple comparison (R=0.44, uncorrected p<0.001, respectively). **: FDR corrected p<0.05. TPOmid.R: Right middle temporal pole.

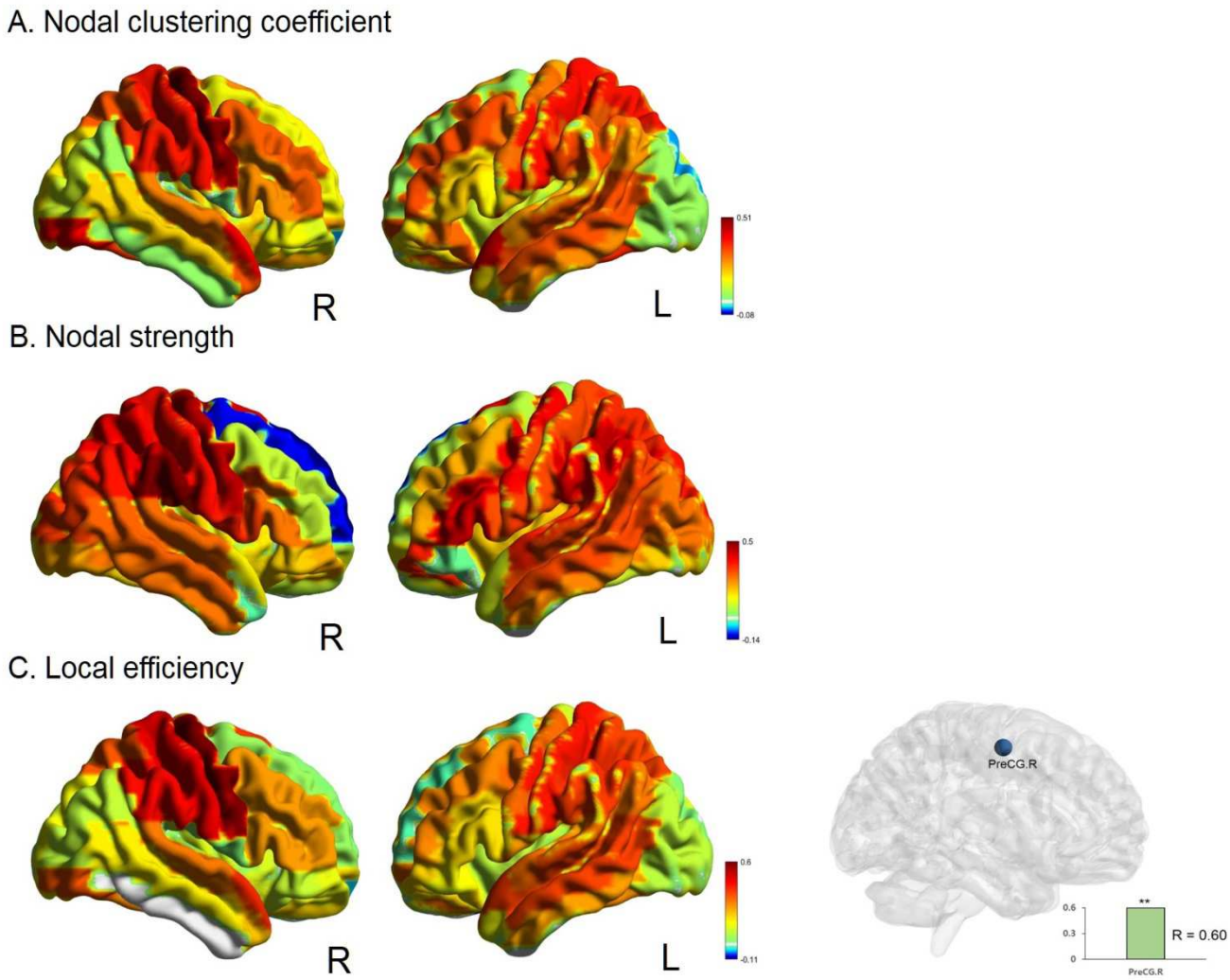

Supplementary Figure 4. Associations between the CR marker and local graph parameters

in normal aging. **A.** Nodal clustering coefficient **B.** Nodal strength **C.** Local efficiency. Each left and middle figures represent the raw correlation maps between the CR marker and each graph parameter in right (R) and left (L) hemisphere. The scale bar shows the range of correlation values. The right figure in **C** shows the significant ROI (PreCG.R) correlated with the CR marker in local efficiency. In nodal clustering coefficient (**A**), PreCG.R had the highest correlation with the CR marker among all nodes, but did not survive for multiple comparison (R=0.51, uncorrected p=0.002). In nodal strength (**B**), PreCG.R had the second-highest correlation with the CR marker following Rt. supramarginal gyrus (R=0.50, uncorrected p=0.003). **: FDR corrected p<0.05. PreCG.R: Right precentral gyrus.

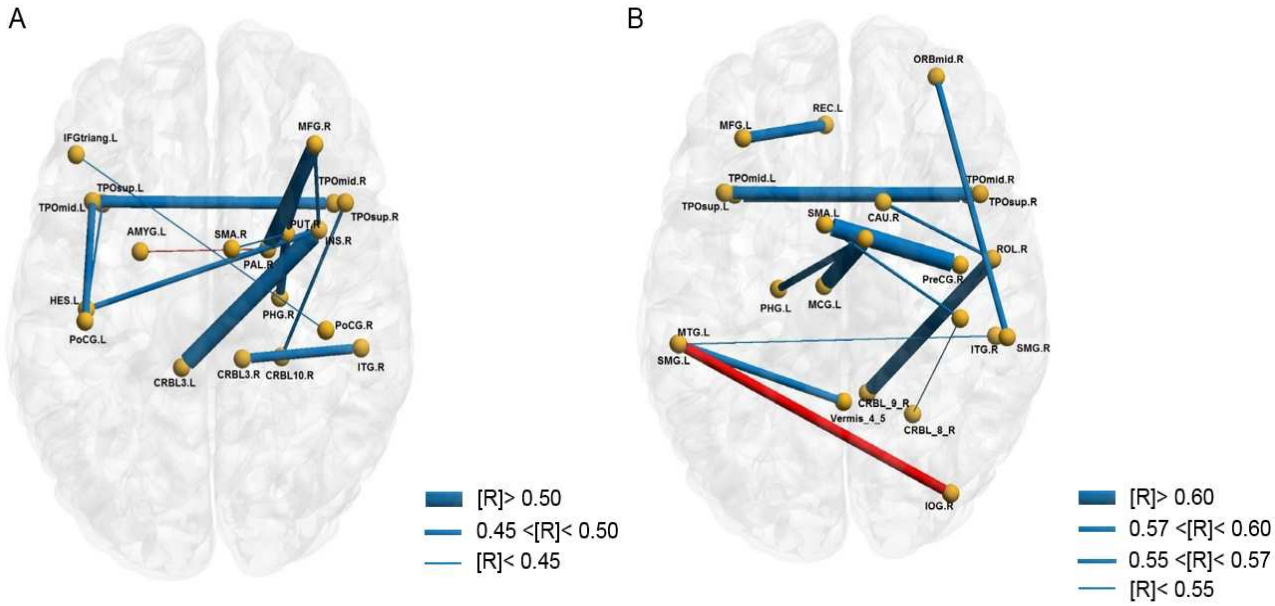

Supplementary Figure 5. Relationships between functional connectivity (FC) and the CR marker in respective AD spectrum and normal aging. **A.** FC showing significant correlation with the CR marker in AD spectrum (p<0.001). **B.** FC showing significant correlation with the CR marker in normal aging (p<0.001). Edges of positive correlation are presented in blue and negative edges are red. The thickness of edge indicates correlation coefficient between each FC and the CR marker (R). The full names of abbreviations in significant ROIs are listed in Supplementary Table 1.

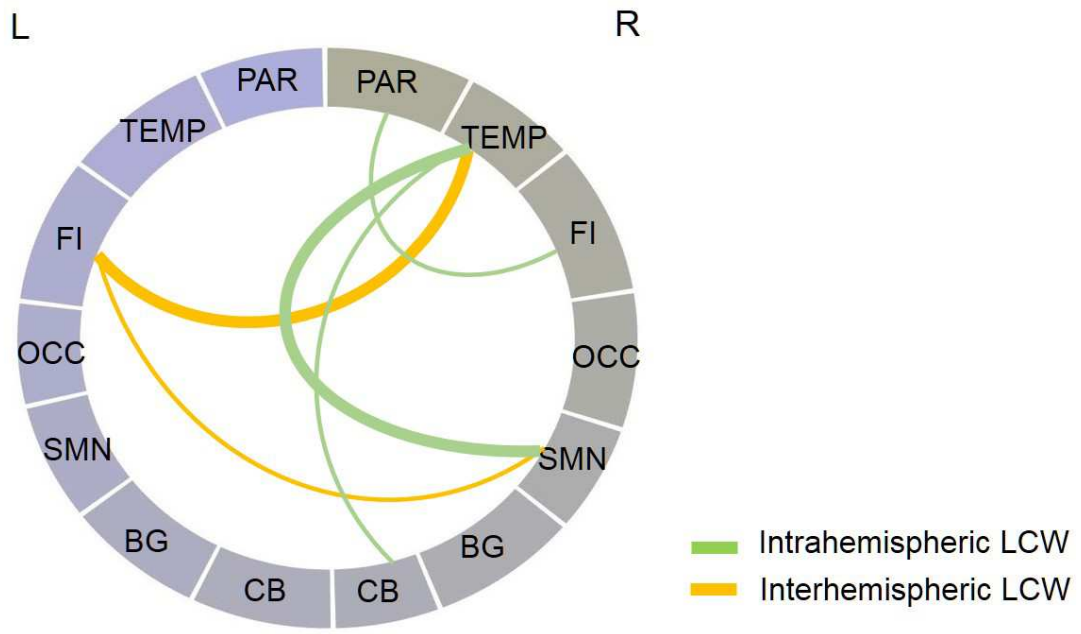

Supplementary Figure 6. Correlation between the CR marker and lobar connectivity weight (LCW). The green lines denote intrahemispheric LCW correlated with the CR marker and yellow lines indicate interhemispheric LCW correlated with the CR marker. The two thicker lines denote significant LCWs in correlation with the CR marker at uncorrected $p<0.005$ (left frontoinsular – right temporal: 0.35, right temporal – sensorimotor: 0.32, respective correlation coefficient) and others show significance at $p<0.01$. FI= fronto-insular, PAR= parietal, BG= basal ganglia, OCC= occipital, TEMP= temporal, SMN= sensorimotor.